

Modeling Volatility-Based Aerosol Phase State Predictions in the Amazon Rainforest

Quazi Z. Rasool, Manish Shrivastava,* Mega Octaviani, Bin Zhao, Brian Gaudet, and Ying Liu

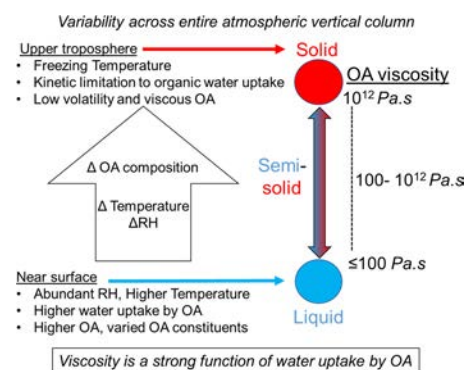
ABSTRACT: Organic aerosol (OA) is a complex matrix of various constituents—fresh (primary organic aerosols—POA) and aged via oxidation (secondary organic aerosols—SOA), generated from biogenic, anthropogenic, and biomass burning sources. The viscosity of OA can be critical in influencing new particle formation, reactive uptake processes that impact evaporation growth kinetics, and the lifetime of particles in the atmosphere. This work utilizes a well defined relationship between volatility and viscosity for pure compounds, which we incorporated within the Weather Research and Forecasting Model coupled to chemistry (WRF Chem) to simulate the phase state and viscosity of bulk OA during the dry to wet transition season (September–October) in the Amazon rainforest during 2014. Our simulations indicate spatial and temporal heterogeneity in aerosol phase state often not captured by global scale models. We show the strong role of water associated with organic aerosol (w_s) as the dominant factor that can be used to quantitatively estimate OA viscosity. Analysis of WRF Chem simulations across the entire atmospheric column indicates a strong inverse log linear relationship between w_s and OA viscosity with a correlation coefficient approaching 1, in the background and biomass burning influenced conditions. At high altitudes where relative humidity (RH) and temperatures are low, our simulations indicate that OA exists in a semisolid /solid like phase state, consistent with previous studies. OA hygroscopicity is strongly correlated (ca. -0.8) with OA viscosity at RH ca. 30–50%, but this RH range is found mostly at low OA concentrations and the middle troposphere (ca. 6–10 km altitudes) in our simulated domain. OA hygroscopicity is uncorrelated with viscosity at higher RH (near surface) and lower RH (upper troposphere) regimes. At the urban site near surface, where day–night differences in RH are significant, RH is found to drive the phase state. At the background forested site near surface, where day–night RH differences are small, biomass burning influenced OA is semisolid and a significant OA associated with background conditions is liquid like. Simulations indicate a long tail of OA viscosity frequency distributions extending in the semisolid/solid regimes over background biogenic influenced conditions due to the role of low volatility OA components such as monoterpene oxidation products.

KEYWORDS: *phase state, secondary organic aerosols, volatility, viscosity, glass transition temperature, phase transitions, water uptake by organic aerosols, Amazon rainforest*

■ INTRODUCTION

Secondary organic aerosols (SOA) formed from the condensation of lower volatility products resulting from the oxidation of volatile organic compounds (VOCs) of varying volatilities from biogenic and anthropogenic sources, contribute between 30 and 70% to total global atmospheric aerosol mass.^{1–3} Yet their physicochemical properties are poorly understood.⁴ In addition, OA consisting of SOA and primary organic aerosol (POA) uptakes water as a function of its composition and hygroscopicity (defined by κ_{org} for overall OA or κ_{org} for OA constituents, which varies between 0.05 and 0.2^{5–8}).^{9–11} Aerosol water acts as a plasticizer for atmospheric aerosol and is strongly dependent on relative humidity (RH). As RH increases, the water content associated with organics also increases to maintain equilibrium with the gas phase.^{12,13} In addition to RH, aerosol liquid water also varies in the atmosphere with OA composition dependent hygroscopicity.¹⁴

One of the most uncertain physicochemical properties of OA is its phase state (as in liquid, semisolid, or solid) quantified by the viscosity of the matrix composed of organic aerosol and the water associated with it. Viscosity can be directly converted to diffusion rates for organic molecules using the Stokes–Einstein equation, which has been shown to work well for gas phase organic molecules diffusing through liquid particles and large particles.^{15–17} However, application of the Stokes–Einstein equation in cases of small molecules has limitations, and it may



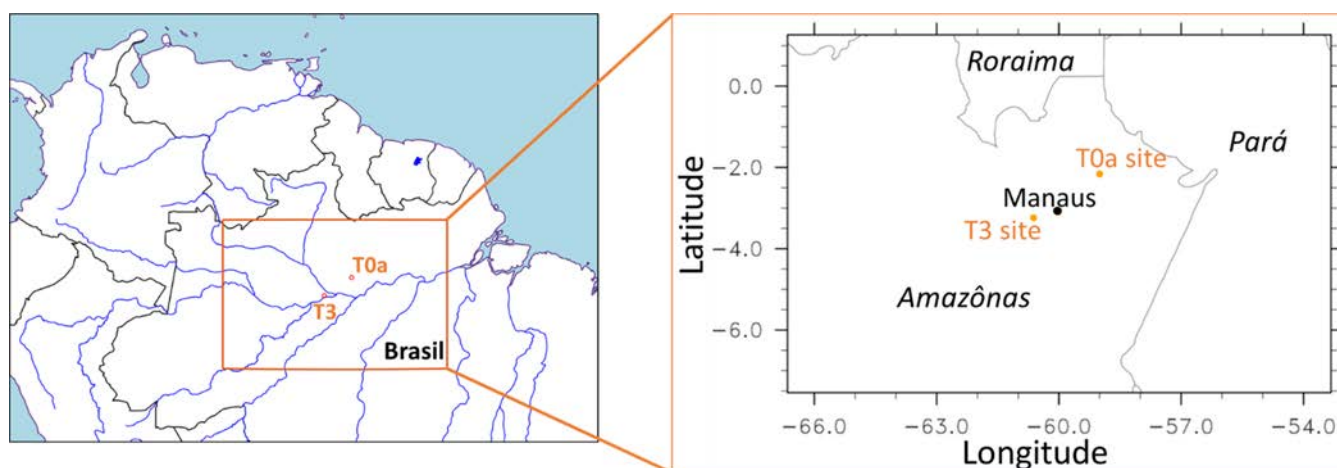


Figure 1. WRF Chem modeling domain (orange) for the simulations during 19 September–2 October 2014. Orange markers on the inset indicate the GoAmazon2014/5 sites: T0a ATTO forest tower site (~150 km northeast upwind of Manaus) and T3 (~70 km downwind of Manaus) in Amazônas, Brazil.

also underestimate the diffusion rates of gas phase organic molecules in a highly viscous matrix.^{15,18}

In the aqueous particle phase, OA could lose mass through heterogeneous reactions such as hydrolysis as in the case of organic nitrates^{19,20} or gain mass by reactive uptake of gas phase species, e.g., isoprene epoxydiols (IEPOX), to the particle phase.^{21,22} These heterogeneous reactions depend on the phase state of aerosol, i.e., whether it is liquid, semisolid, or solid.²³ For instance, if particles are in the liquid phase, bulk particle phase diffusional resistance for condensing species such as IEPOX gas would be negligible, allowing these particles to grow rapidly through the uptake of IEPOX. In contrast, solid particles would exhibit significant in particle diffusional resistance and would shut off reactive uptake of IEPOX. In between the two extremes of liquid and solid particles, OA exhibits a range of viscosities that could be classified as semisolid (e.g., like peanut butter or honey) behavior, which slows down the reactive uptake and growth of particles, which could also affect aerosol optical properties,^{24,25} their atmospheric lifetimes, and long range transport.^{26–29} Aerosol phase state, viscosity, and bulk diffusivity affect the gas particle partitioning of organics and growth of aerosols to sizes where they act as cloud condensation nuclei (CCN).³⁰

Diffusion rates and therefore aerosol phase state are critical to predict the reactivity and photochemistry,^{31–37} growth rates and size distribution dynamics,³⁸ cloud condensation ability,³⁹ and ice nucleating ability of SOA particles.^{40–42} The focus in this work is on SOA phase state given recent advances in understanding volatility based viscosity production of organics.⁴³ Most current atmospheric models assume SOA particles as liquid like homogeneous particles throughout the atmosphere, which could be inaccurate, especially in cold and dry regions of the atmosphere, e.g., in the middle and upper tropospheres, where OA is mostly semisolid/solid.⁴⁴ In addition, even near the surface, particles in wildfire plumes have been shown to be in semisolid state even under high RH (~70%) conditions over the Amazon, likely due to their differing composition compared to background biogenic SOA.^{45–47} Without a comprehensive treatment of aerosol phase state and viscosity, its effects on SOA formation and particle size distribution cannot be represented in predictive models of atmospheric chemistry, climate, and air quality.^{1,30,48–52}

This work implements a new framework within the Weather Research and Forecasting Model coupled to chemistry (WRF Chem) for predicting the dynamic variations in OA viscosity as a function of its volatility and oxygen to carbon ratio (O:C), as detailed in the subsequent section. The Amazon rainforest is one of the unique terrestrial locations on the earth where OA transitions between pre industrial like and polluted conditions due to the influence of the Manaus city plume during wet season and biomass burning during the dry season.⁵³ For our analyses, we chose a time period in the dry to wet transition IOP2 season of GoAmazon2014/5 as it provides a unique opportunity to study the impact on aerosol phase state, i.e., viscosity, of the interactions of biomass burning emissions in central Amazonia with the pre industrial natural biogenic emissions of the tropical rainforest. Besides the composition of the matrix of organics originating from the mixing of pollution plumes with the natural background, other prevailing factors such as ambient temperature and RH, which drives aerosol liquid water content, also perturb aerosol phase state and viscosity both spatially and temporally.^{9,47}

■ METHODS

Modeling Study Domain Description. The modeling domain used in this study is centered around the city of Manaus in the central Amazonian region of Brazil (Figure 1). The modeling domain extends from -7.54275° to 1.26334° from south to north and -66.6571° to -53.3249° across west to east. The study period for which results will be presented spans 19 September–2 October 2014, corresponding to the dry to wet transition season IOP2 of the GoAmazon2014/5 experiment.⁵⁴ Manaus, an isolated urban region with a population of over 2 million, situated at the confluence of the Black River (Rio Negro) to its north with the Solimões river to its south, which together form the Amazon river, is surrounded by forested region in its vicinity (Figure 1). GoAmazon2014/5 experiments focused on two sites located downstream and upstream of Manaus, namely, “T3” and “T0a”, respectively (inset of Figure 1). We focused on these two sites for analyses of factors affecting modeled aerosol viscosity and leverage the unique chemical interactions between the background air of the Amazon basin and pollution from mostly biomass burning prevailing in dry or

dry to wet transition seasons for the central Amazonian region.^{55,56}

“T3” (3.2133° S, 60.5987° W) at Manacapuru, 70 km to the southwest of Manaus, is a pasture site surrounded by forest.⁵⁴ Previous modeled flow trajectories of the pollution plume from Manaus are shown to intercept the T3 site about 60% of the time in dry or dry to wet transition seasons driven by westerlies.⁵⁵ Analyses of GoAmazon2014/5 T3 site observational data sets also characterized pollution episodes to be occurring in the range of 15–30% of the observed time.^{57,58} Site “T0a” (2.1466° S, 59.0050° W), which refers to the Amazonian Tall Tower Observatory (ATTO), is located 150 km to the northeast of Manaus and served as references for background conditions in relation to T3.⁵⁹ The T0a site is upwind of Manaus, with only occasional transport of urban pollution to it.^{59,60} It should be noted that during dry or dry to wet transition season (IOP2), both T3 and T0a sites are affected by local and long range transport of biomass burning emissions brought in by westerlies.⁵⁶ Moreover, the proportional increase of deforested area—i.e., % of average area deforested to total vegetation cover during 2007–2014—was the highest in municipalities around Manaus among all municipality regions of Brazil.⁶¹ This high deforestation rate around Manaus has been strongly correlated with slash and burn fires to clear out forested land for agricultural or industrial purposes.^{62,63} This makes Manaus an appropriate center of the study domain to also look at the impact of biomass burning with respect to background conditions on aerosol phase state.

Phase State Prediction: Volatility-Based Glass-Transition Temperatures and Viscosity. Volatility and viscosity have been established as interconnected and critical properties of OA, both of which impact processes such as gas particle partitioning and heterogeneous reactions, new particle formation and growth pathways, and OA size distribution.^{51,64–67} We refer to the viscosity of total OA matrix, which includes POA, SOA, and aerosol water associated with these organics, and denote it as η_{org} . OA can exist in liquid ($\eta_{\text{org}} < 10^2$ Pa·s), semisolid ($10^2 \leq \eta_{\text{org}} < 10^{12}$ Pa·s), and glassy or amorphous solid ($\eta_{\text{org}} \geq 10^{12}$ Pa·s) phase states, depending on the chemical composition of the OA matrix along with ambient temperature (T) and RH.⁶⁷

Glass-Transition Temperature of Organic Aerosol Constituents. In this work, η_{org} is determined based on the glass transition temperature of various constituents of the organic aerosol matrix ($T_{\text{g,org}}$), which is simply the temperature at which transition between semisolid and amorphous solid phase state occurs.¹² For liquids, the ratio of $T_{\text{g,org}}$ to the ambient temperature (T) is less than 0.8, and this ratio increases as the viscosity of the OA matrix increases. When this ratio is equal to 1, a complete transition from semisolid to glass phase occurs, and the OA matrix is solid at ratios greater than 1. More recently $T_{\text{g,org}}$ has been predicted using semiempirical parameterizations using molar mass (M) and atomic O:C ratio of different OA species⁵² or their elemental composition,⁶⁸ but these approaches depend on ascertaining the molecular structure for OA compounds or their functional group specificity such as number of carbon, hydrogen, oxygen, nitrogen, and sulfur,⁶⁹ which are often not available for all compounds constituting OA.

In this work, we implement a recent parametrization of $T_{\text{g,org}}$ based on volatility distributions and O:C measurements of different ambient OA species.⁴³ Volatility distribution of the OA matrix varies as a function of its composition and implicitly accounts for the molecular and functional differences of various

POA and SOA components. Li et al.⁴³ established the strong dependence of $T_{\text{g,org}}$ on pure compound saturation concentration (C^*), i.e., volatility of 2325 organic compounds including CH, CHO, CHON (organic nitrate), and CHOS (organosulfate) compounds, where literature derived measured or estimated $T_{\text{g,org}}$ and C^* were compiled from previous studies. Li et al.⁴³ however concluded that the O:C ratio (as a parameter) does not significantly affect $T_{\text{g,org}}$ predictions, particularly for compounds with low O:C ratios. The fitted $T_{\text{g,org}}$ based on these findings were used in this work as represented in eq 1, as a first step to represent the volatility–viscosity relationship.

$$T_{\text{g,org}} = \begin{cases} 289.10 - 16.5(\log_{10} C^*) - 0.29(\log_{10} C^*)^2 \\ \quad + 3.23(\text{O} : \text{C}_{\text{OA}})(\log_{10} C^*), & \text{if } \text{O} : \text{C}_{\text{OA}} \\ > 0 \\ 288.70 - 16.5(\log_{10} C^*) - 0.33(\log_{10} C^*)^2 \\ \quad , & \text{else} \end{cases} \quad (1)$$

$T_{\text{g,org}}$ showed a weak dependence on the O:C ratio of the overall OA mixture (O:C_{OA}) when both O:C and volatility were used. Hence, an alternative equation with $T_{\text{g,org}}$ only depending on volatility (C^*) can be adopted when the O:C ratio is not available (eq 1). O:C_{OA} is estimated as weighted sum of different species specific O:C ratios based on the mass fractions of these species in total OA. In this study, we either directly specify O:C ratios of various OA components from the literature or estimate it based on their hygroscopicity, i.e., κ_{org} from the literature for OA species using eq 2, which holds only for CH and CHO compounds.^{14,70}

$$\kappa_{\text{org}} = 0.14(\text{O} : \text{C}) + 0.03 \quad (2)$$

These O:C ratios for various OA species, which are used in this work, are presented in Supporting Information Table S1. Our results show that $T_{\text{g,org}}$'s of different ambient OA species relevant to this work, determined from their respective volatility and O:C ratio, exhibit a strong inverse relation with volatility and no significant dependence on O:C ratio (Figure S1).

In Figure S1, volatility is expressed empirically as an effective saturation concentration in $\mu\text{g m}^{-3}$ on a logarithmic coordinate (i.e., $\log_{10} C^*$) and glass transition temperatures of different organic aerosol species are plotted as a function of C^* and O:C ratio. The glass transition temperature for intermediate volatility organic compounds (IVOC: $300 < C^* < 3 \times 10^6 \mu\text{g m}^{-3}$)^{71,72} would be <250 K. For semivolatile organic compounds (SVOC: $0.3 < C^* < 300 \mu\text{g m}^{-3}$),^{71,72} $T_{\text{g,org}}$ is ~ between 255 and 295 K, whereas it is higher than 300 K for low volatility organic compounds (LVOC; $3 \times 10^{-4} < C^* < 0.3 \mu\text{g m}^{-3}$).^{71,72} Extremely low volatility organic compounds (ELVOC: $3 \times 10^{-8} < C^* < 3 \times 10^{-4} \mu\text{g m}^{-3}$) and ultralow volatility organic compounds (ULVOC: $C^* < 3 \times 10^{-8} \mu\text{g m}^{-3}$), which are mostly products of autoxidation or dimerization such as low volatility monoterpene SOA and IEPOX SOA dimers in cloud phase critical to CCN production,^{72,73} are characterized by higher $T_{\text{g,org}}$'s. ULVOC and ELVOC fall in the $T_{\text{g,org}}$ range of ca. 330–415 K.^{74,75} Hence, as the mass fractions of low volatility constituents in the OA mixture increase especially under low RH conditions, the particles tend to approach a solid phase state.

Viscosity Calculation for Organic Aerosol Mixture. Combined glass transition temperature ($T_{\text{g,mix}}$) for OA and aerosol water associated with them, which would eventually be

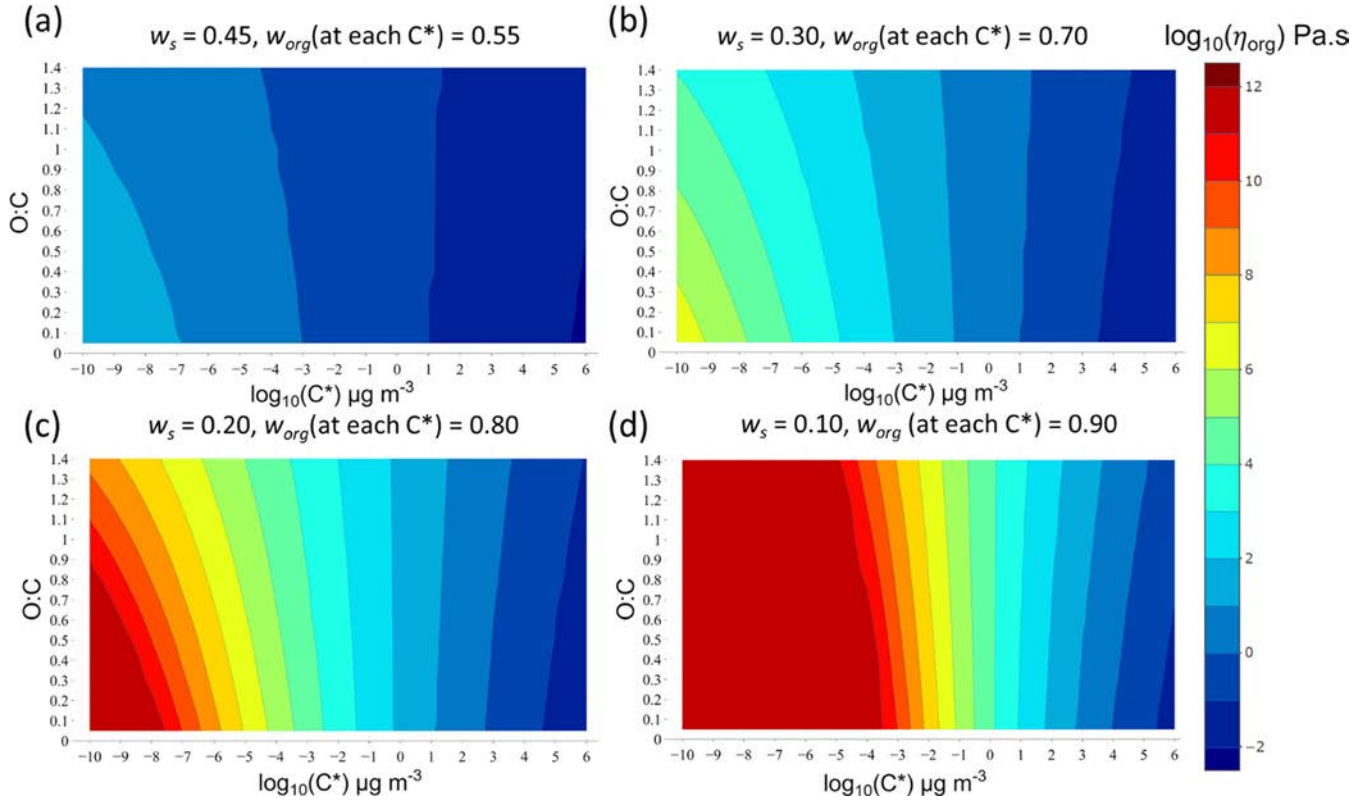


Figure 2. Box model predictions showing the logarithm of the viscosity of organic aerosols $\log_{10}(\eta_{\text{org}})$ (color bar) as a function of volatility (X axis, $\log_{10}C^*$) and O:C ratio (Y axis) at a temperature of 300 K under (a) wet conditions with 45% organic water fraction, w_s , (b, c) intermediate ranges at 20 and 30% w_s , respectively, and (d) dry conditions (10% w_s) during the GoAmazon2014/5 campaign dry to wet transition season. The isopleths correspond to the $\log_{10}(\eta_{\text{org}})$ calculated using our viscosity prediction framework, as described in the text.

used to predict viscosity, is calculated using a modified version of the Gordon–Taylor mixing rule^{68,76} (eq 3) with the $T_{\text{g,org}}$ of each OA constituent making up aerosol mixture calculated using eq 1 described in the previous section.

$$T_{\text{g,mix}} = \frac{\left(w_s T_{\text{g,w}} + \frac{1}{K_{\text{GT}}} \left(\sum w_{\text{org}} T_{\text{g,org}} \right) \right)}{w_s + \frac{1}{K_{\text{GT}}} \left(\sum w_{\text{org}} \right)} \quad (3)$$

where $T_{\text{g,w}}$ is the glass transition temperature of water¹² (~ 136 K), $T_{\text{g,org}}$ is the glass transition temperatures (K) of different organic OA constituents making up the aerosol mixture, K_{GT} is the Gordon–Taylor constant, which is assumed to be 2.5 based on Koop et al.,¹² w_{org} refers to the mass fractions of different OA species constituting the total organic aerosol mixture, w_s is the mass fraction of water associated with organic aerosols, which depends on the hygroscopicity of OA, and $w_s + \sum w_{\text{org}}$ make up all of the organics + associated water adding up to 1, as given in eq 4.

$$w_s = 1 - \left(\sum w_{\text{org}} \right) \equiv \frac{\text{mc}_{\text{aerosol water associated with organics}}}{\text{mc}_{\text{aerosol water associated with organics}} + \sum \text{mc}_{\text{all organics}}} \quad (4)$$

In eq 4, mc refers to mass concentrations and w_s serves as a major modulator of aerosol phase state, which depends on RH and hygroscopicity of different OA constituents, as observed in recent field measurements.^{77–79} These findings now also are the basis of modeling aerosol water content in contemporary atmospheric models.

OA exhibits a solid like glassy phase state when $T_{\text{g,mix}} > T$, corresponding to a maximum limit to η_{org} as 10^{12} Pa.s. A liquid or semisolid phase state occurs when $T_{\text{g,mix}} < T$. The variability in η_{org} with ambient T being below or above $T_{\text{g,mix}}$ can be as high as 8 orders of magnitude.⁸⁰ Thus, $T_{\text{g,mix}}$ can be used to determine when aerosols are in a highly viscous glassy state, a semisolid state, or a liquid state, analogous to the phase state demarcations as per η_{org} ranging between 100 and 10^{12} Pa.s.^{81–83} The η_{org} value is calculated using a modified Vogel–Tamman–Fulcher equation^{68,84} and related to $T_{\text{g,mix}}$ with experimentally fitted parameters and a fragility parameter D (eqs 5–7). We follow the recommendation of Gervasi et al.⁸⁵ to assign $D = 10$, except when $T_{\text{g,mix}} > T$. For $T_{\text{g,mix}} > T$, a fragility parameter of $D = 30$ was found to accurately estimate the pure component viscosity, and, by extension, the mixture viscosity.⁸⁵

$$\log_{10}(\eta_{\text{org}}) = -5 + 0.434 \frac{T_0 D}{T - T_0} \quad (5)$$

$$T_0 = \frac{39.17 T_{\text{g,mix}}}{D + 39.17} \quad (6)$$

$$D = \begin{cases} 30, & \text{if } T_{\text{g,mix}} > T \\ 10, & \text{else} \end{cases} \quad (7)$$

where T is the ambient temperature (K), T_0 is an experimentally fitted parameter that varies as a function of $T_{\text{g,mix}}$ and the fragility parameter D represents whether the phase state transition between liquid to semisolid and subsequently solid can be quick. Smaller D values indicate that viscosity is more

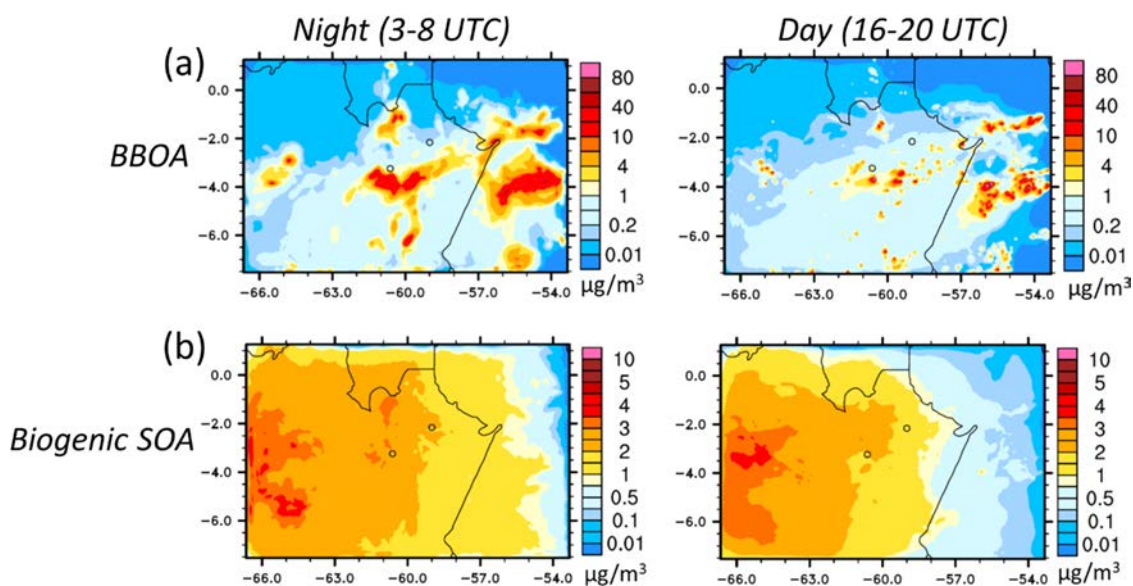


Figure 3. WRF Chem simulated (a) biomass burning OA (BBOA = BB POA + BB SOA) and (b) total biogenic SOA from isoprene SOA, terpene SOA (monoterpenes SOA + sesquiterpene SOA), and IEPOX SOA, averaged during the simulation period of 19 September–2 October 2014 for nighttime (3–8 UTC) (left) and daytime (16–20 UTC) (right), at surface. The hollow black markers refer to T3 (near the center of domain and the urban Manaus region) and T0a (background site northeast of Manaus) sites. (Locations of T3 and T0a sites are marked in the inset panel of Figure 1).

sensitive to temperature change (fragile behavior), while larger D values indicate that viscosity is less sensitive to temperature change (steady or Arrhenius behavior).⁶⁸

WRF-Chem Setup and Updates for Modeling Volatility-Based Viscosity. We used the community regional Weather Research and Forecasting Model coupled to chemistry (WRF Chem version 4.2) for generating modeling results in this study.^{86,87} Our configuration of the WRF Chem model (summarized in Table S1) includes the updates found in Zhao et al.⁷² and Shrivastava et al.⁵³ but applied to our WRF Chem version 4.2 model for a domain covering the central Amazon basin with a grid spacing of 10 km (Figure 1). The configuration used 45 vertical layers from the surface to the 50 hPa pressure level, with layers more closely spaced at lower altitudes. We adapted in WRF Chem the two dimensional volatility basis set (2D VBS),⁷⁵ as implemented in Zhao et al.,^{72,73} which represents the temperature dependent oxidation of monoterpenes by a 17 bin VBS with C^* ranging from 10^{-10} to $10^6 \mu\text{g m}^{-3}$ (Figure S1). In addition, updates on hygroscopicity and O:C of various OA constituents making up the aerosol mixture, relevant to the viscosity prediction framework in our WRF Chem model, are detailed in Table S2. Gas phase chemistry is coupled with the MOSAIC (Model for Simulating Aerosol Interaction and Chemistry) aerosol module.⁸⁸ The eight aerosol size bins used in the modeling framework were 0.039–0.078, 0.078–0.156, 0.156–0.312, 0.312–0.624, 0.624–1.25, 1.25–2.5, 2.5–5.0, and 5–10 μm . We used an anthropogenic emission inventory for the Amazon region from Shrivastava et al.,⁵³ while biomass burning emissions were from 2014 Quick Fire Emissions Database (QFED v2.5 <https://portal.nccs.nasa.gov/datashare/ies/aerosol/emissions/QFED/v2.5r1/0.1/QFED/>) inventory and were coupled to the Freitas plume rise model. WRF Chem used online biogenic emissions calculated using the Model of Emissions of Gases and Aerosols from Nature (MEGAN v2.1)⁸⁹ coupled within the land surface scheme of Community Land Model Version 4 (CLM4) in WRF Chem Version 4.2.⁹⁰ The physics parametrizations of WRF Chem were all the same as in Zhao et al.⁷² (Table S1). WRF

Chem simulated ambient temperature and RH at the T3 surface site, averaged for the modeling period, agreed well with the corresponding observations for both daytime and nighttime (see Figure S2 in the Supporting Information for details).

RESULTS AND DISCUSSION

Box Modeling of Viscosity as a Function of Volatility and O:C. To derive insights into the various parameters affecting viscosity calculations, we designed idealized simulations within a 0D box model, besides the regional scale 3D WRF Chem modeling, discussed later. For each fixed and prescribed value of OA water content, we varied $\log_{10}(C^*)$ —ranging from -10 to 6 (in intervals of 1) and O:C ranging from 0 to 1.4 (in intervals of 0.1) (Figure 2). Viscosity, i.e., η_{org} , is calculated from eq 5 based on glass transition temperature, calculated using eq 1.⁴³ These calculations are done at a mean ambient temperature of 300 K as found near surface in dry to wet transition GoAmazon2014/5 season considered in this work. Our results demonstrate that η_{org} is inversely correlated with C^* (Figure 2).

When OA water fraction is relatively high (Figure 2a, $w_s = 0.45$) typically associated with near surface high RH conditions over the Amazon, the box model predicts that OA is liquid with viscosity ($\leq 100 \text{ Pa}\cdot\text{s}$), regardless of composition (represented by different saturation concentration, C^*). Thus, at higher w_s values (Figure 2a), RH is the dominant factor affecting aerosol viscosity and OA composition weakly affects simulated viscosity. However, under the low and intermediate RH conditions prevailing at higher altitudes over the Amazon, volatility and O:C ratio (governed by OA composition) strongly affect simulated viscosity in addition to RH, as shown in Figure 2b–d.

At lower RH (Figure 2d, $w_s = 0.10$), simulations predict that extremely low volatility and low volatility organic compounds (ELVOCs and LVOCs with $C^* < 1 \times 10^{-3} \mu\text{g m}^{-3}$) will be solid, while semivolatile organic compounds (SVOCs, $1 \times 10^{-3} < C^* < 100 \mu\text{g m}^{-3}$) will exist as semisolids. Intermediate volatility organic compounds (IVOCs, $C^* > 100 \mu\text{g m}^{-3}$) are predicted to be liquids, but their contributions to OA will be much smaller

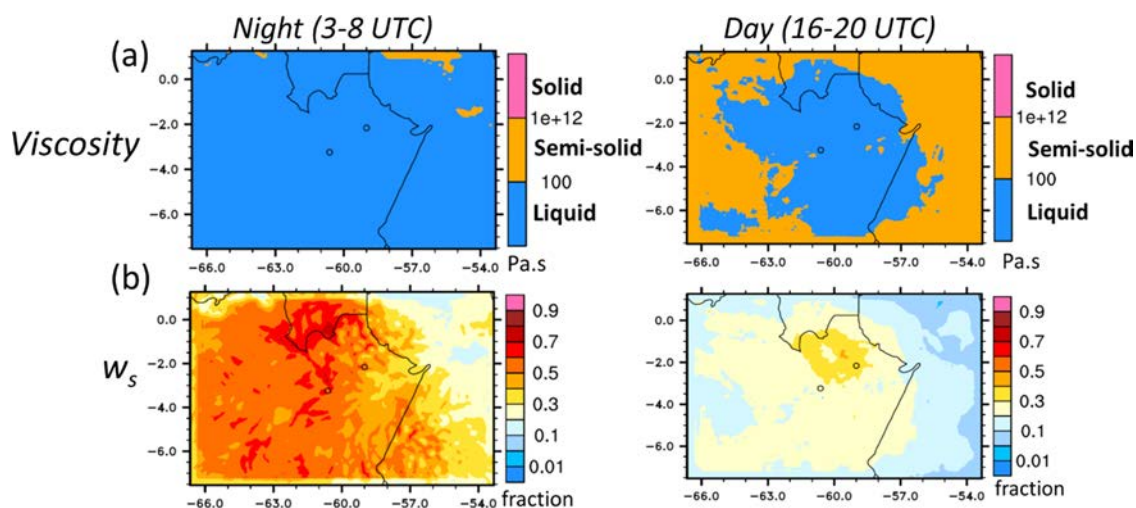


Figure 4. Same as Figure 3 but for (a) OA viscosity, η_{org} and (b) organic water fraction, w_s .

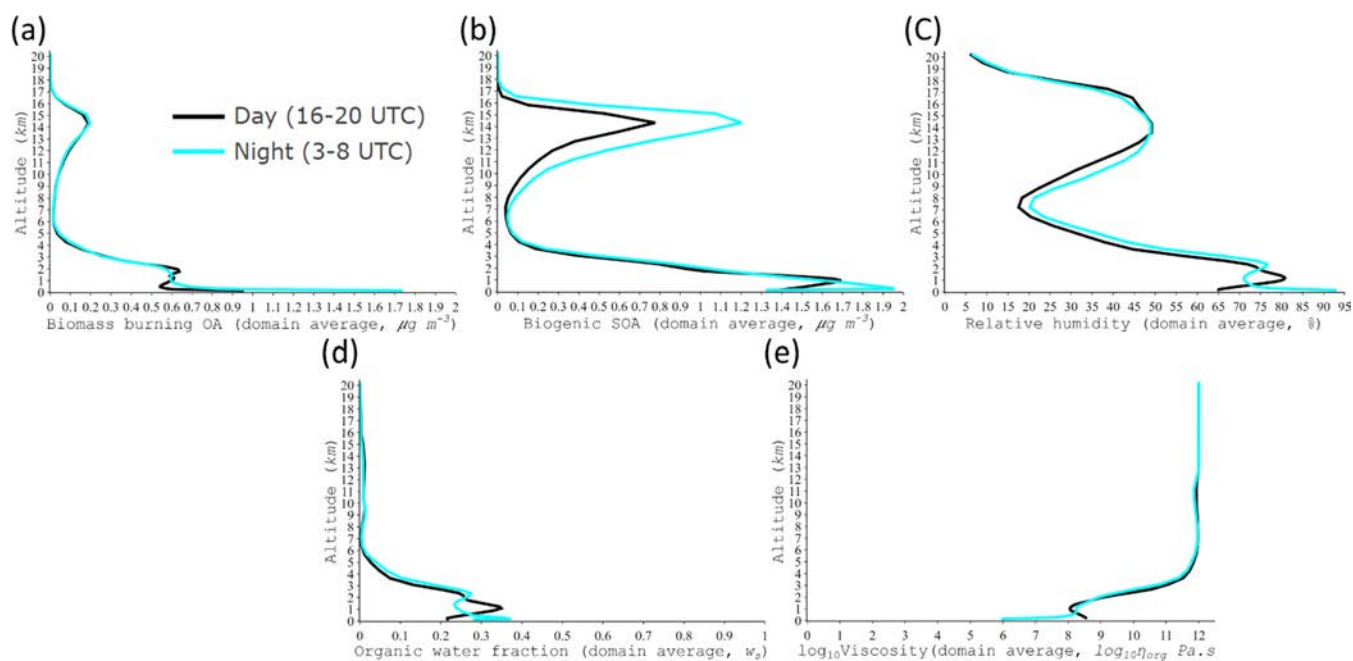


Figure 5. WRF Chem simulated vertical profiles for daytime (16–20 UTC) and nighttime (3–8 UTC). (a) Biomass burning OA (BB POA + BB SOA), (b) total biogenic SOA, (c) relative humidity (RH %), (d) organic water fraction, w_s , and (e) OA viscosity, η_{org} averaged across the modeling domain during the simulation period of 19 September–2 October 2014.

than SVOCs and LVOCs at 300 K, since most IVOCs will partition to gas phase except in highly concentrated plumes like in the core of wildfires. In comparison, at higher RH (Figure 2a, $w_s = 0.45$), all species (ELVOCs, LVOCs, SVOC, IVOCs) are predicted to be liquids. However, at cold temperatures (below 273 K) prevalent at higher altitudes in the atmosphere, ELVOCs and LVOCs are predicted to approach semisolid/solid phases at $w_s = 0.45$ (Figure S3a,c), while under dry conditions ($w_s = 0.10$) and low temperatures, even SVOCs can exist as semisolids/solids (Figure S3b,d). For intermediate RH conditions (Figure 2b,c, $w_s = 0.20$ or 0.30), ELVOCs and LVOCs can remain in semisolid phases, but these exist in the solid phase for lower RH conditions (Figure 2d).

In most regimes (Figures 2 and S3), the O:C ratio has minimal impacts on viscosity, as indicated by nearly vertical isopleths of viscosity. Greater impacts of O:C are predicted at $\log_{10}(C^*) > 5$ for lower organic water fraction (Figure 2d) and

at $\log_{10}(C^*) < -5$ for higher and intermediate organic water fractions (Figure 2a–c). The variation of modeled viscosity with O:C ratio exhibits different trends for IVOC and ELVOC/ULVOC. While simulated viscosity increases slightly with O:C for IVOC under dry conditions, consistent with previous studies,^{12,79,91} it decreases slightly as the O:C ratio increases for ELVOC/ULVOC compounds, consistent with Li et al.⁴³ However, the impact of O:C on η_{org} is much smaller than C^* . Thus, our box modeling simulations show that C^* under dry or relatively intermediate conditions and organic water fraction are the main factors governing aerosol phase state. Consistently, Champion et al.⁹² found that higher fractions of ELVOCs and LVOCs in SOA were associated with an increased viscosity, while O:C did not affect it significantly. In subsequent sections, we apply this parameterization within WRF Chem to assess variations in OA phase state over the central Amazonian region.

Influence of Biomass Burning. WRF Chem simulations show large biomass burning OA (BBOA) mass concentrations in the regions of central and southwest Amazonia. Our simulations also indicate that primary BBOA mass concentrations are much greater than biomass burning SOA. Simulated BBOA concentrations are much higher and cover a larger area during the nighttime (3–8 UTC) compared to the daytime (16–20 UTC) averaged during 19 September–2 October 2014 for 0–4 km altitude range (Figures 3a and S4). The German High Altitude and Long Range Research Aircraft (HALO) campaign also observed high BBOA during several days during this time.⁹³

Simulations predict higher BBOA concentrations at 12 km than at 6 km (Figure S4). This agrees with HALO flight observations showing enhanced BBOA particle concentrations after being lofted to the upper troposphere (8–15 km) by deep convection, as removal processes are inefficient at these altitudes.⁹⁴ Biogenic SOA is also enhanced in the upper troposphere, i.e., 12 km compared to 6 km (Figure S5), because of monoterpene oxidation products that govern new particle formation in the Amazonian free troposphere, as documented in Zhao et al.⁷² Anthropogenic OA is more concentrated (0.1–1 $\mu\text{g m}^{-3}$ on average for simulation period) around the T3 site corresponding to obvious peak urban emission activities originating from Manaus, which is adjacent to the T3 site.

However, overall, anthropogenic OA (not shown) is quite small across the domain ($<0.1 \mu\text{g m}^{-3}$ outside the urban pollution plume on average for simulation period) in comparison to BBOA and biogenic SOA (Figure 3a,b). This is consistent with the measurements by high resolution time of flight aerosol mass spectrometer (AMS) data and positive matrix factorization analyses for the GoAmazon2014/15 dry to wet transition season (15 August–15 October 2014).⁵⁶ Hence, in addition to biogenic SOA, biomass burning is a substantial OA component, which governs OA phase state predictions. Especially near surface, within wildfire plumes, BBOA could be up to an order of magnitude higher than biogenic SOA (Figure 3a,b). From the average mass concentration trends of BBOA for the modeling domain (Figure 3a), we characterize background where BBOA $<0.2 \mu\text{g m}^{-3}$ and biomass burning plumes where BBOA $>2 \mu\text{g m}^{-3}$. Thus, classifying our simulated domain within two categories, in plume and background, we compare the simulated distribution of OA viscosity for Central Amazonia.

Viscosity and Its Strong Dependence on Organic Water Fraction. WRF Chem simulations show a strong inverse dependence of aerosol phase state quantified by OA viscosity, η_{org} , on organic water fraction, w_s , for both nighttime (3–8 UTC) and daytime (16–20 UTC) (Figures 4, S6, and S7). For nighttime at surface and daytime at 2 km, even when higher biomass burning OA mass concentrations are present (Figure 5a), OA exists in the liquid phase ($\eta_{\text{org}} \leq 100 \text{ Pa}\cdot\text{s}$) due to high w_s (0.3–0.7) prevailing at these instances relative to other altitudes (Figures 4 and 5d,e). Simulated BBOA concentrations are much higher near surface at nighttime compared to the daytime (Figure 5a). Higher BBOA loadings at nighttime along with higher nighttime near surface RH (Figure 5c) cause the simulated viscosity to be lower at nighttime compared to daytime (Figure 5e). Variability in RH governs the variabilities in both w_s and η_{org} (Figures 4, S6–S8, and 5c–e), with higher RH resulting in higher w_s and liquid like OA phase and vice versa for solid phase. Thus, our simulations indicate that high w_s (and high RH) is the dominant factor determining the phase state of BBOA, although BBOA has been reported to be associated with

semisolid/solid phase,⁴⁶ which likely prevails under low RH conditions.

Simulated BBOA exists as semisolid ($100 \text{ Pa}\cdot\text{s} < \eta_{\text{org}} < 10^{12} \text{ Pa}\cdot\text{s}$) at low w_s (below 0.3, associated with low RH regions) from surface to 4 km altitudes in both daytime and nighttime (Figures S6 and S7). The semisolid behavior of BBOA, especially under low RH conditions, can mostly be explained by its low volatility. In this work, we assume primary BBOA has C^* of $0.1 \mu\text{g m}^{-3}$, but its volatility can be 1–2 orders of magnitude lower since tar balls in BB plumes are known to have low volatility.^{95–97} If BBOA is of lower volatility in the ELVOC/LVOC range, our box modeling simulations show that it will be semisolid in both low and intermediate ranges of w_s (Figure 2b,c).

Altitude Dependence of OA Phase State. Our simulations show that OA exists in a solid amorphous phase state at high altitudes $>6 \text{ km}$, where w_s is often lower than $\sim 5\%$ (Figures 5d,e, S6, and S7). A semisolid phase state mostly occurs around 4 km corresponding to $w_s \sim 5\text{--}25\%$, and OA exists in a liquid phase state near surface (0–2 km), where w_s is much higher than 25%. In summary, semisolid or solid aerosol phase state is more prevalent in the middle and upper tropospheres (Figures S6 and S7), consistent with previous studies.⁵² An amorphous solid OA phase state ($\eta_{\text{org}} \geq 10^{12} \text{ Pa}\cdot\text{s}$) persists even in the presence of some RH and aerosol water at altitudes 6–12 km during both daytime and nighttime (Figures 5c,e, S8, and S9) due to low temperatures (temperatures drop 50° below freezing point of water at 12 km altitude). The particles are practically frozen at these low temperatures and exist as solids, and there are strong limitations to particle phase diffusion within the highly viscous OA matrix in the middle and upper tropospheres.⁴⁸

Figure S10 indicates that $T_{\text{g,mix}}:T$ ratio is a reasonable indicator of aerosol phase state. Regions with $T_{\text{g,mix}}:T$ ratio >1 correspond exactly to an amorphous solid OA phase state with $\eta_{\text{org}} \geq 10^{12} \text{ Pa}\cdot\text{s}$ (Figures S6, S7, and S10), as per the Koop et al.¹² criteria that characterize $T_{\text{g,mix}}:T$ as an indicator of when aerosol reaches perfect glassy state. The threshold value of $T_{\text{g,mix}}:T$ between liquid and semisolid phases is calculated to be ~ 0.7748 (Figures S6, S7, and S10) using fragility parameter $D = 10$ and ambient temperature (eqs 5–7). The transitional $T_{\text{g,mix}}:T$ boundary between liquid and semisolid aerosol phase state has been approximated to 0.8 in previous global scale studies.⁵²

Simulated Viscosity Trends at T3 and T0a GoAmazon2014/5 Sites. *Organic Water Fraction w_s : An Excellent Indicator of OA Viscosity.* We analyzed the multiday variations of aerosol phase state metrics (η_{org} and $T_{\text{g,mix}}:T$ ratio) at the T3 and T0a sites corresponding to GoAmazon2014/5, for the period of 19 September–2 October 2014 across altitudes of 0–15 km. Aerosol phase state metrics at T3 and T0a GoAmazon2014/5 sites are referring to gridded model outputs at those sites. The methodology used for extracting these site specific model outputs is based on extracting data from the two nearest neighbor grid cells in each direction. w_s has the strongest inverse correlation with viscosity, ca. -0.99 at both T0a and T3 sites during daytime and nighttime (Figure 6), and this trend between w_s and viscosity is seen for the whole domain. Our simulations show a linear relationship between $\log_{10}(\eta_{\text{org}})$ and $\log_{10}(w_s)$, with an ~ 1 correlation coefficient (Figure 6). Direct measurements of the viscosity of OA are difficult especially in the field. However, using the linear relationship shown in Figure 6, the viscosity of OA can be readily estimated from ambient field measurements of OA mass concentrations, hygroscopicity, and ambient RH.

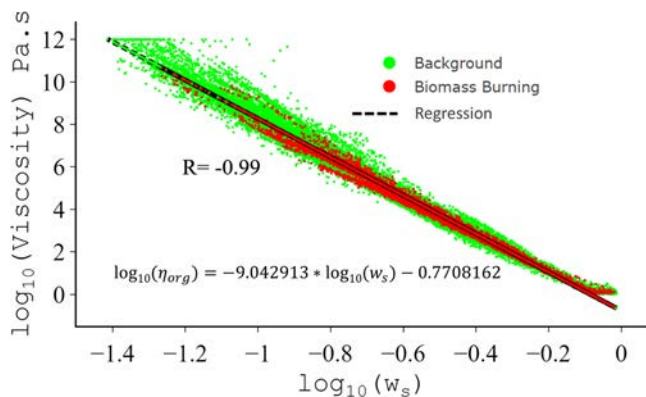


Figure 6. WRF Chem simulated trends of organic aerosol water fraction, w_s (x axis), vs viscosity (η_{org} Pa·s, y axis) on \log_{10} – \log_{10} scale for both T0a and T3 sites across the entire atmospheric vertical column during 19 September–2 October 2014. The black dashed line represents the linear regression fit. “Background” and “Biomass burning” events are represented by green and red markers, respectively.

Site specific analyses (Figures S11 and S12) confirm the dominant role of organic water fraction with its higher value (Figures S11c and S12c) resulting in the tendency of OA phase state shifting to liquid behavior (Figures S11a and S12a). Near the surface, w_s is higher during nighttime at T3 compared to T0a, and the converse for daytime (Figures S11c and S12c). These trends in w_s explain the difference in the simulated η_{org} and $T_{g,\text{mix}}:T$ ratio near the surface (Figures S11a,b and S12a,b). In the middle and upper tropospheres, as the temperature drops below the freezing point of water, viscosity increases, and the OA phase state is predicted to be predominantly amorphous solid at >6 km at both T3 and T0a sites (see the [Altitude Dependence of](#)

[OA Phase State](#) section). The $T_{g,\text{mix}}:T$ ratio explains the transitions between solid and semisolid regime and coincides with almost negligible w_s at higher altitudes (Figures S11 and S12). This ratio reaches a maximum around 6–10 km and within regions of the atmosphere at the lowest RH, e.g., at altitudes >12 km (Figures S8, S11b, and S12b). Simulations indicate a higher organic water fraction at 0.5–1.5 km relative to the surface due to higher RH for daytime (16–20 UTC) (Figure S8b, see the higher RH in 2 km map relative to surface map at both T0a and T3). Thus, analyzing WRF Chem simulations, we show that organic water fraction w_s is a key unifying parameter combining the effects of ambient RH, OA composition, volatility, and hygroscopicity of OA on the viscosity of OA, supporting its role as a predictor of OA viscosity, but this finding needs experimental validation. The accuracy of w_s estimates depends on accurate quantification of OA loadings, hygroscopicity, and RH in the atmosphere.

Role of Organic Aerosol Composition in Viscosity Predictions at T3 and T0a Sites. From WRF Chem simulations, we calculate and compare cumulative distribution function (CDF) of the aerosol viscosity (η_{org}) at T3 and T0a sites from background versus in plume conditions (Figures 8a and 9a). These distributions directly correspond to CDFs of organic water fraction w_s (Figures 8b and 9b), i.e., lower w_s corresponds to higher η_{org} and vice versa. WRF Chem simulations reinforce our findings from box model simulations that OA associated water (w_s) is a strong determinant of aerosol phase state. As these analyses are at surface, RH variability can also explain the trends in aerosol viscosity (Figures 7–9). Normalized probability distribution function (PDF) of RH can explain the probability distributions of OA viscosity, same as w_s (Figures S13 and S14).

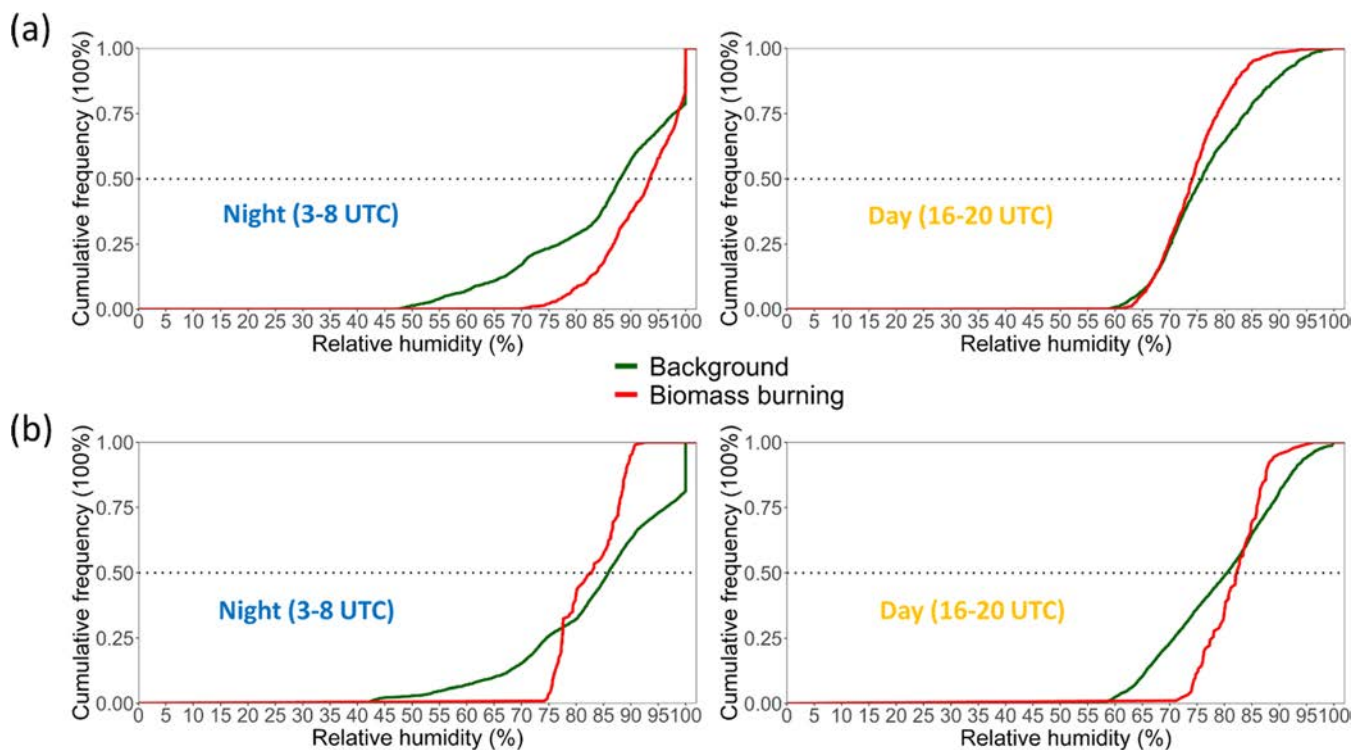


Figure 7. WRF Chem simulated cumulative distribution functions (CDFs) of relative humidity (RH %) for (a) T3 (near Manaus) site and (b) T0a (ATTO, northeast of Manaus) site, for nighttime (3–8 UTC, left) and daytime (16–20 UTC, right). CDFs for background and biomass burning influenced regions are shown separately.

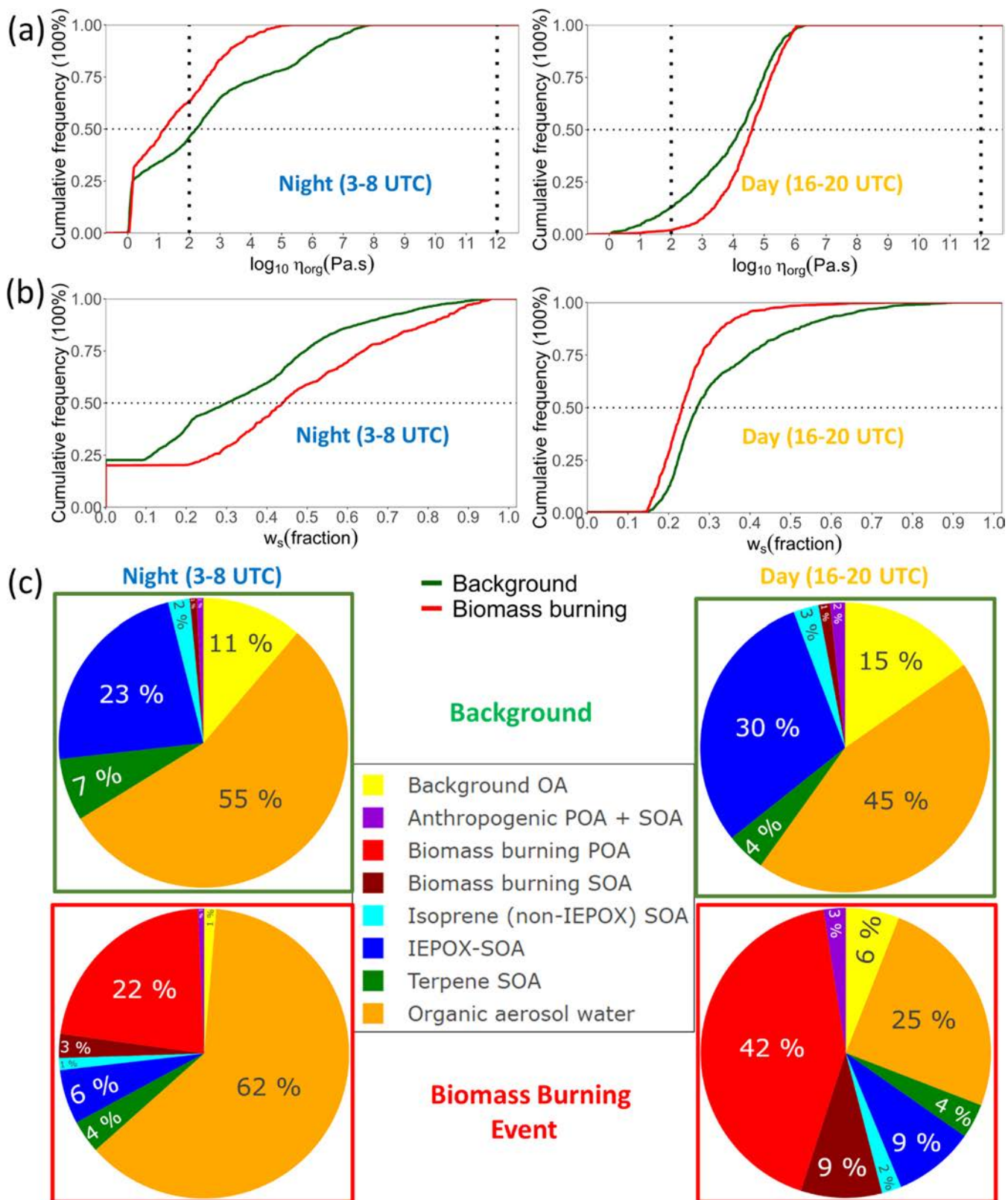


Figure 8. WRF Chem simulated quantities derived at T3 (near Manaus) site background and biomass burning at surface for (a) cumulative distributions of OA viscosity on logarithmic scale, $\log_{10} (\eta_{\text{org}} \text{ Pa}\cdot\text{s})$, (b) cumulative distributions of organic water fraction, w_s , and (c) mean OA composition, for nighttime (3–8 UTC, left) and daytime (16–20 UTC, right).

At the T3 site, the mean and median surface RH and w_s are higher during nighttime compared to daytime (Figures S11c, 7a, and 8b) within both background and biomass burning

influenced regimes. Calculated CDFs indicate a 50% probability that $(\log_{10} \eta_{\text{org}})$ will take values below 2, i.e., in the liquid phase at nighttime (Figure 8a). In contrast, during the daytime most of

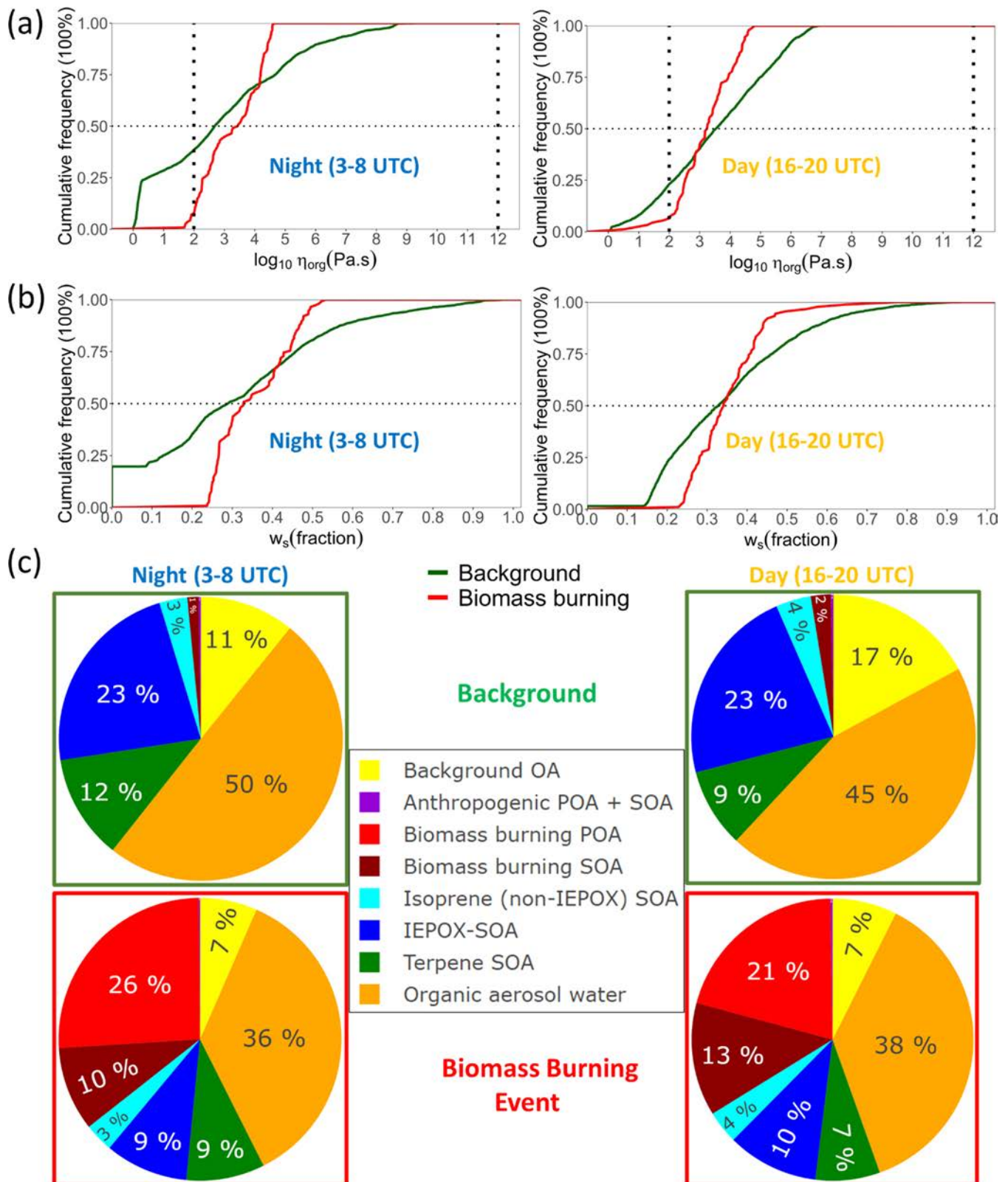


Figure 9. Same as Figure 8 but for the T0a (ATTO, northeast of Manaus) site.

the ($\log_{10} \eta_{\text{org}}$) values are predicted to be in the semisolid regime ($\log_{10} \eta_{\text{org}} > 2$) (Figure 8a).

During the daytime within biomass burning plumes, BBOA comprises >50% of total OA with w_s averaging ~ 0.25 near surface (Figure 8c). Biomass burning plumes are also associated with slightly lower RH than the background conditions (Figure

7a). This results in a minuscule population of liquid particles during the daytime biomass burning events, even lower than that in the background (Figure 8a). This is qualitatively consistent with findings from Bateman et al.^{9,45,46} for the T3 site where semisolid particles with a high rebound fraction were prevalent in biomass burning events. Background OA consists of different

OA types with a range of volatilities including IEPOX SOA, terpene SOA, and background OC (ELVOCs, LVOCs, and SVOCs), whereas primary BBOA is mostly LVOCs. This explains the longer tail of CDFs of background at higher viscosities compared to biomass burning events (Figure 8a). During nighttime, biomass burning plumes are associated with overall higher RH ranges (ca. 75–95%) compared to background conditions (ca. 50–95%, and 25th quantile at <75%) (Figure 7a). This explains the more liquid like phase associated with biomass burning plumes in the nighttime relative to background conditions, which exhibit semisolid OA phase (Figure 8a). PDFs of RH, w_s , and $\log_{10} \eta_{\text{org}}$ at both T3 and T0a sites at both nighttime and daytime concur with the above inferences (Figures S13 and S14), as discussed below.

At the T0a ATTO site, the mean and median surface RHs are similar during both daytime and nighttime within biomass burning plumes and background ranging ca. 80–84% (Figure 7b), as ATTO is situated in a pristine rainforest.⁵⁹ At T0a, the contribution of BBOA is smaller than that at the T3 site since T3 is downwind of Manaus around which most of biomass burning events occur with T0a being upwind.⁵⁴ Median behavior (50% cumulative distributions) at T0a for RH and w_s do not differ much, consequently resulting in similar viscosity profiles (Figures 7b and 9a,b). Biomass burning events for both daytime and nighttime predominantly result in semisolid particles OA compared to background cases, which have significant liquid aerosol population (Figure 9a). Biomass burning events at T0a also exhibit ca. 8–15% lower w_s than in background cases on average (Figure 9c) even though mean and median ambient RH are similar in either case. This can be explained by: (1) a narrower and often lower range of hygroscopicity for BBOA influenced regions compared to the background biogenic SOA, which has higher hygroscopicity (Table S2, further discussed in subsequent section), and (2) a narrower range of RH associated with biomass burning events (ca. 75–90%), compared to a wider RH range associated with background conditions in both daytime and nighttime. The lower simulated w_s in biomass burning influence compared to background regions explains the corresponding differences in the probability distributions of viscosity at T0a (Figures 7b and 9a).

The CDF of ($\log_{10} \eta_{\text{org}}$) exhibits a long tail extending in semisolid/solid regimes for background OA at T0a (Figure 9a). This is due to a broader range of w_s for background conditions at T0a during both daytime and nighttime (Figure 9b). Greater contributions of a predominantly monoterpene derived SOA source (that includes ELVOCs and LVOCs) and aged background OA from boundary conditions contributing to OA at T0a cause a long tail extending toward solid like viscosities in the background compared to biomass burning events (Figure 9c).

Role of Organic Aerosol Hygroscopicity in Viscosity Predictions. Overall, OA hygroscopicity, i.e., κ_{org} , affects the calculated viscosity through its influence on w_s . Simulated κ_{org} varies with OA composition and ranges from 0.04 to 0.15 (Table S2). Figure S15b shows that within the RH range of 30–50% at the T0a background site, over the entire atmospheric vertical column, viscosity is highly sensitive to changes in κ_{org} (correlation ca. -0.8). Simulated viscosity increases by 3 orders of magnitude from $\log_{10}(\eta_{\text{org}}) \sim 8.5$ (semisolid like pitch or tar) to 11.5 (solid) as κ_{org} decreases from 0.12 to 0.1. At lower RHs (<30%), the aerosol phase state remains semisolid (more viscous than tar)/solid, i.e., $\log_{10}(\eta_{\text{org}})$ ca. 10–12 (Figure S15a), while at higher RH (>70%, Figure S15c), OA

approaches a liquid like phase. Thus, under both low and high RH conditions, OA viscosity does not correlate with κ_{org} . OA composition and associated κ_{org} are correlated with OA viscosity only in the intermediate RH range of 30–50%, where minor changes in κ_{org} by 0.02 were associated with transition of OA from semisolid to solid phase state. Our results suggest that accurately predicting κ_{org} is more important in regions of the atmosphere at intermediate RH ranges (30–50% RH) compared to the lower/higher RH regimes. However, it is important to note that the simulated RH ca. 30–50% mostly exists in the middle troposphere at ca. 6–10 km altitude (Figure 5c), where WRF Chem simulates much smaller OA concentrations (<0.1 $\mu\text{g m}^{-3}$) compared to the surface at both T0a and T3 sites (Figures S4 and S5).

■ CONCLUSIONS

This study provides unique insight into the spatial and temporal heterogeneities of aerosol phase state. We show that aerosol water associated with OA is the primary driver of aerosol viscosity. While direct measurements of OA viscosity are difficult in the field, we show that viscosity can be easily estimated from its linear relationship with w_s on a log scale. w_s is a unifying parameter that combines several variables: ambient RH, OA composition, volatility, and hygroscopicity of OA, and therefore emerges as the key predictor of OA viscosity. OA composition, hygroscopicity, and ambient RH are often available from field measurements and can be used to quantitatively estimate w_s and hence OA viscosity, as shown in this study. We show that OA phase state strongly varies with altitude in the atmosphere. With increasing altitude, as temperature and RH decrease, OA exists in a glassy or amorphous solid phase. At the T3 site in central Amazonia, day–night differences in RH cause OA populations to be more liquid during night and semisolid/solid during the daytime. These trends are similar in background and biomass burning influenced regimes at T3. In contrast, at the background T0a site where day–night differences in RH are small, biomass burning causes most aerosol populations to be in the semisolid/solid phases, whereas in the background, a significant fraction of OA population is liquid like. In addition, background OA exhibits a longer tail extending toward higher viscosities approaching solid phases compared to biomass burning influenced regimes due to wider ranges of background OA composition, volatility, and hygroscopicity. Near surface, high RH (ca. 70–80%), and OA mass concentrations are key factors affecting OA viscosity, while in the upper troposphere (10–14 km altitude), OA is mostly solid due to low temperature (~ 225 K) and RH ($\sim 40\%$). Therefore, OA hygroscopicity is not correlated with simulated viscosity near surface and in the upper troposphere. At intermediate RH ranges (ca. 30–50%), prevailing in the middle troposphere (6–10 km altitudes), simulated OA hygroscopicity shows a strong linearly inverse correlation with OA (ca. -0.8); however, OA concentrations are much smaller in the middle troposphere. It should be noted that hygroscopicity and water uptake by OA constituents could be impacted by uncertainty in the miscibility among various constituents of OA and the mixing state of aerosol.⁹⁸ Recent work indicated that this uncertainty in miscibility and mixing state of OA constituents could modestly impact model predicted OA.⁹⁹ Hence, future work should try to account for these uncertainties especially in global scale modeling that may deal with varied OA composition profiles and ambient conditions.

This implementation of volatility based viscosity calculation in our regional atmospheric WRF Chem modeling framework offers promising prospects for investigating the uncertain relationships between phase state and OA growth/evolution in the atmosphere, which have implications for aerosol–cloud interactions and climate.

■ ASSOCIATED CONTENT

● Supporting Information

The Supporting Information is available free of charge at <https://pubs.acs.org/doi/10.1021/acsearthspacechem.1c00255>.

WRF Chem model configuration (Table S1); other modeling updates for the representation of SOA formation and OA properties including the viscosity calculation framework presented in the text, which we implemented in WRF Chem (Table S2); WRF Chem performance against the observed temperature and relative humidity at the T3 site near Manaus (Figure S2); box modeling results (Figures S1 and S3); WRF Chem predicted OA viscosity and related parameters influencing it for the modeling domain (Figures S4–S10) at both T0a (ATTO) and T3 (near Manaus) locations (Figures S11–S15); and references (PDF)

■ AUTHOR INFORMATION

Corresponding Author

Manish Shrivastava – Atmospheric Sciences and Global Change Division, Pacific Northwest National Laboratory, Richland, Washington 99352, United States; orcid.org/0000-0002-9053-2400; Email: manishkumar.shrivastava@pnnl.gov

Authors

Quazi Z. Rasool – Atmospheric Sciences and Global Change Division, Pacific Northwest National Laboratory, Richland, Washington 99352, United States; orcid.org/0000-0001-6274-6236

Mega Octaviani – Atmospheric Sciences and Global Change Division, Pacific Northwest National Laboratory, Richland, Washington 99352, United States; Present Address: Institute of Meteorology and Climate Research, Department of Troposphere Research, Karlsruhe Institute of Technology, Eggenstein Leopoldshafen 76344, Germany

Bin Zhao – Atmospheric Sciences and Global Change Division, Pacific Northwest National Laboratory, Richland, Washington 99352, United States; Present Address: State Key Joint Laboratory of Environmental Simulation and Pollution Control, School of Environment, Tsinghua University, Beijing 100084, China

Brian Gaudet – Atmospheric Sciences and Global Change Division, Pacific Northwest National Laboratory, Richland, Washington 99352, United States

Ying Liu – Atmospheric Sciences and Global Change Division, Pacific Northwest National Laboratory, Richland, Washington 99352, United States

Complete contact information is available at: <https://pubs.acs.org/doi/10.1021/acsearthspacechem.1c00255>

Author Contributions

Q.Z.R. and M.S. designed the study. Q.Z.R. and M.S. implemented the modeling development, with contributions from M.O. and B.Z. Q.Z.R. performed the box modeling. M.S.

performed the WRF Chem model simulations. Y.L. processed emissions for WRF Chem model simulations. Q.Z.R. performed analysis and visualization. Q.Z.R. and M.S. wrote the manuscript, with contributions from B.Z., B.G., and M.O. M.S. supervised the overall project.

Notes

The authors declare no competing financial interest.

■ ACKNOWLEDGMENTS

This research was supported by the U.S. Department of Energy (DOE) Office of Science, Office of Biological and Environmental Research (BER) through the Early Career Research Program and DOE BER's Atmospheric System Research (ASR) program. Pacific Northwest National Laboratory (PNNL) is operated for DOE by the Battelle Memorial Institute under contract no. DE A05 76RLO1830. Computational resources for the simulations were provided by EMSL (a DOE Office of Science User Facility sponsored by the Office of Biological and Environmental Research located at PNNL). Funding for data collection at the ground sites was provided by the Atmospheric Radiation Measurement (ARM) Climate Research Facility, a U.S. Department of Energy Office of Science user facility sponsored by the Office of Biological and Environmental Research.

■ REFERENCES

- (1) Hallquist, M.; Wenger, J. C.; Baltensperger, U.; Rudich, Y.; Simpson, D.; Claeys, M.; Dommen, J.; Donahue, N.; George, C.; Goldstein, A.; et al. The formation, properties and impact of secondary organic aerosol: current and emerging issues. *Atmos. Chem. Phys.* **2009**, *9*, 5155–5236.
- (2) Kanakidou, M.; Seinfeld, J.; Pandis, S.; Barnes, I.; Dentener, F. J.; Facchini, M. C.; Dingenen, R. V.; Ervens, B.; Nenes, A.; Nielsen, C.; et al. Organic aerosol and global climate modelling: a review. *Atmos. Chem. Phys.* **2005**, *5*, 1053–1123.
- (3) Jimenez, J. L.; Canagaratna, M.; Donahue, N.; Prevot, A.; Zhang, Q.; Kroll, J. H.; DeCarlo, P. F.; Allan, J. D.; Coe, H.; Ng, N.; et al. Evolution of organic aerosols in the atmosphere. *Science* **2009**, *326*, 1525–1529.
- (4) Nozière, B.; Kalberer, M.; Claeys, M.; Allan, J.; D'Anna, B.; Decesari, S.; Finessi, E.; Glasius, M.; Grgic, I.; Hamilton, J. F.; et al. The molecular identification of organic compounds in the atmosphere: state of the art and challenges. *Chem. Rev.* **2015**, *115*, 3919–3983.
- (5) Huff Hartz, K. E.; Rosenørn, T.; Ferchak, S. R.; Raymond, T. M.; Bilde, M.; Donahue, N. M.; Pandis, S. N. Cloud condensation nuclei activation of monoterpene and sesquiterpene secondary organic aerosol. *J. Geophys. Res.: Atmos.* **2005**, *110* (D14), DOI: 10.1029/2004JD005754.
- (6) VanReken, T. M.; Ng, N. L.; Flagan, R. C.; Seinfeld, J. H. Cloud condensation nucleus activation properties of biogenic secondary organic aerosol. *J. Geophys. Res.* **2005**, *110* (D7), DOI: 10.1029/2004JD005465.
- (7) Petters, M. D.; Kreidenweis, S. M. A single parameter representation of hygroscopic growth and cloud condensation nucleus activity. *Atmos. Chem. Phys.* **2007**, *7*, 1961–1971.
- (8) King, S. M.; Rosenoern, T.; Shilling, J. E.; Chen, Q.; Martin, S. T. Increased cloud activation potential of secondary organic aerosol for atmospheric mass loadings. *Atmos. Chem. Phys.* **2009**, *9*, 2959–2971.
- (9) Bateman, A. P.; Bertram, A. K.; Martin, S. T. Hygroscopic influence on the semisolid to liquid transition of secondary organic materials. *J. Phys. Chem. A* **2015**, *119*, 4386–4395.
- (10) Hildebrandt Ruiz, L.; Paciga, A.; Cerully, K.; Nenes, A.; Donahue, N.; Pandis, S. Formation and aging of secondary organic aerosol from toluene: changes in chemical composition, volatility, and hygroscopicity. *Atmos. Chem. Phys.* **2015**, *15*, 8301–8313.

- (11) Massoli, P.; Lambe, A.; Ahern, A.; Williams, L.; Ehn, M.; Mikkilä, J.; Canagaratna, M.; Brune, W.; Onasch, T.; Jayne, J. et al. Relationship between aerosol oxidation level and hygroscopic properties of laboratory generated secondary organic aerosol (SOA) particles. *Geophys. Res. Lett.* **2010**, *37* (24), DOI: 10.1029/2010GL045258.
- (12) Koop, T.; Bookhold, J.; Shiraiwa, M.; Pöschl, U. Glass transition and phase state of organic compounds: dependency on molecular properties and implications for secondary organic aerosols in the atmosphere. *Phys. Chem. Chem. Phys.* **2011**, *13*, 19238–19255.
- (13) Nguyen, T. K. V.; Zhang, Q.; Jimenez, J. L.; Pike, M.; Carlton, A. G. Liquid water: Ubiquitous contributor to aerosol mass. *Environ. Sci. Technol. Lett.* **2016**, *3*, 257–263.
- (14) Pye, H. O. T.; Murphy, B. N.; Xu, L.; Ng, N. L.; Carlton, A. G.; Guo, H.; Weber, R.; Vasilakos, P.; Appel, K. W.; Budisulistiorini, S. H.; Surratt, J. D.; Nenes, A.; Hu, W.; Jimenez, J. L.; Isaacman VanWertz, G.; Misztal, P. K.; Goldstein, A. H. On the implications of aerosol liquid water and phase separation for organic aerosol mass. *Atmos. Chem. Phys.* **2017**, *17*, 343–369.
- (15) Price, H. C.; Mattsson, J.; Murray, B. J. Sucrose diffusion in aqueous solution. *Phys. Chem. Chem. Phys.* **2016**, *18*, 19207–19216.
- (16) Chenyakin, Y.; Ullmann, D. A.; Evoy, E.; Renbaum Wolff, L.; Kamal, S.; Bertram, A. K. Diffusion coefficients of organic molecules in sucrose–water solutions and comparison with Stokes–Einstein predictions. *Atmos. Chem. Phys.* **2017**, *17*, 2423–2435.
- (17) Ullmann, D. A.; Hinks, M. L.; Maclean, A. M.; Butenhoff, C. L.; Grayson, J. W.; Barsanti, K.; Jimenez, J. L.; Nizkorodov, S. A.; Kamal, S.; Bertram, A. K. Viscosities, diffusion coefficients, and mixing times of intrinsic fluorescent organic molecules in brown limonene secondary organic aerosol and tests of the Stokes–Einstein equation. *Atmos. Chem. Phys.* **2019**, *19*, 1491–1503.
- (18) Evoy, E.; Maclean, A. M.; Rovelli, G.; Li, Y.; Tsimpidi, A. P.; Karydis, V. A.; Kamal, S.; Lelieveld, J.; Shiraiwa, M.; Reid, J. P.; et al. Predictions of diffusion rates of large organic molecules in secondary organic aerosols using the Stokes–Einstein and fractional Stokes–Einstein relations. *Atmos. Chem. Phys.* **2019**, *19*, 10073–10085.
- (19) Fisher, J. A.; Jacob, D. J.; Travis, K. R.; Kim, P. S.; Marais, E. A.; Chan Miller, C.; Yu, K.; Zhu, L.; Yantosca, R. M.; Sulprizio, M. P.; et al. Organic nitrate chemistry and its implications for nitrogen budgets in an isoprene and monoterpene rich atmosphere: constraints from aircraft (SEAC 4 RS) and ground based (SOAS) observations in the Southeast US. *Atmos. Chem. Phys.* **2016**, *16*, 5969–5991.
- (20) Zare, A.; Romer, P. S.; Nguyen, T.; Keutsch, F. N.; Skog, K.; Cohen, R. C. A comprehensive organic nitrate chemistry: insights into the lifetime of atmospheric organic nitrates. *Atmos. Chem. Phys.* **2018**, *18*, 15419–15436.
- (21) Surratt, J. D.; Chan, A. W.; Eddingsaas, N. C.; Chan, M.; Loza, C. L.; Kwan, A. J.; Hersey, S. P.; Flagan, R. C.; Wennberg, P. O.; Seinfeld, J. H. Reactive intermediates revealed in secondary organic aerosol formation from isoprene. *Proc. Natl. Acad. Sci. U.S.A.* **2010**, *107*, 6640–6645.
- (22) Pye, H. O.; Pinder, R. W.; Piletic, I. R.; Xie, Y.; Capps, S. L.; Lin, Y. H.; Surratt, J. D.; Zhang, Z.; Gold, A.; Luecken, D. J.; et al. Epoxide pathways improve model predictions of isoprene markers and reveal key role of acidity in aerosol formation. *Environ. Sci. Technol.* **2013**, *47*, 11056–11064.
- (23) Schmedding, R.; Rasool, Q. Z.; Zhang, Y.; Pye, H. O. T.; Zhang, H.; Chen, Y.; Surratt, J. D.; Lopez Hilfiker, F. D.; Thornton, J. A.; Goldstein, A. H.; Vizuete, W. Predicting secondary organic aerosol phase state and viscosity and its effect on multiphase chemistry in a regional scale air quality model. *Atmos. Chem. Phys.* **2020**, *20*, 8201–8225.
- (24) Adler, G.; Koop, T.; Haspel, C.; Taraniuk, I.; Moise, T.; Koren, I.; Heiblum, R. H.; Rudich, Y. Formation of highly porous aerosol particles by atmospheric freeze drying in ice clouds. *Proc. Natl. Acad. Sci. U.S.A.* **2013**, *110*, 20414–20419.
- (25) Robinson, C.; Schill, G.; Tolbert, M. Optical growth of highly viscous organic/sulfate particles. *J. Atmos. Chem.* **2014**, *71*, 145–156.
- (26) Bastelberger, S.; Krieger, U. K.; Luo, B.; Peter, T. Diffusivity measurements of volatile organics in levitated viscous aerosol particles. *Atmos. Chem. Phys.* **2017**, *17*, 8453–8471.
- (27) Shrivastava, M.; Lou, S.; Zelenyuk, A.; Easter, R. C.; Corley, R. A.; Thrall, B. D.; Rasch, P. J.; Fast, J. D.; Simonich, S. L. M.; Shen, H.; et al. Global long range transport and lung cancer risk from polycyclic aromatic hydrocarbons shielded by coatings of organic aerosol. *Proc. Natl. Acad. Sci. U.S.A.* **2017**, *114*, 1246–1251.
- (28) Zelenyuk, A.; Imre, D.; Beránek, J.; Abramson, E.; Wilson, J.; Shrivastava, M. Synergy between secondary organic aerosols and long range transport of polycyclic aromatic hydrocarbons. *Environ. Sci. Technol.* **2012**, *46*, 12459–12466.
- (29) China, S.; Alpert, P. A.; Zhang, B.; Schum, S.; Dzepina, K.; Wright, K.; Owen, R. C.; Fialho, P.; Mazzoleni, L. R.; Mazzoleni, C.; et al. Ice cloud formation potential by free tropospheric particles from long range transport over the Northern Atlantic Ocean. *J. Geophys. Res.: Atmos.* **2017**, *122*, 3065–3079.
- (30) Zaveri, R. A.; Easter, R. C.; Shilling, J. E.; Seinfeld, J. Modeling kinetic partitioning of secondary organic aerosol and size distribution dynamics: representing effects of volatility, phase state, and particle phase reaction. *Atmos. Chem. Phys.* **2014**, *14*, 5153–5181.
- (31) Chu, Y.; Chan, C. K. Role of oleic acid coating in the heterogeneous uptake of dimethylamine by ammonium sulfate particles. *Aerosol Sci. Technol.* **2017**, *51*, 988–997.
- (32) Davies, J. F.; Wilson, K. R. Nanoscale interfacial gradients formed by the reactive uptake of OH radicals onto viscous aerosol surfaces. *Chem. Sci.* **2015**, *6*, 7020–7027.
- (33) Gržinić, G.; Bartels Rausch, T.; Berkemeier, T.; Türler, A.; Ammann, M. Viscosity controls humidity dependence of N₂O₅ uptake to citric acid aerosol. *Atmos. Chem. Phys.* **2015**, *15*, 13615–13625.
- (34) Houle, F. A.; Wiegel, A. A.; Wilson, K. R. Predicting Aerosol Reactivity Across Scales: from the Laboratory to the Atmosphere. *Environ. Sci. Technol.* **2018**, *52*, 13774–13781.
- (35) Hinks, M. L.; Brady, M. V.; Lignell, H.; Song, M.; Grayson, J. W.; Bertram, A. K.; Lin, P.; Laskin, A.; Laskin, J.; Nizkorodov, S. A. Effect of viscosity on photodegradation rates in complex secondary organic aerosol materials. *Phys. Chem. Chem. Phys.* **2016**, *18*, 8785–8793.
- (36) Lignell, H.; Hinks, M. L.; Nizkorodov, S. A. Exploring matrix effects on photochemistry of organic aerosols. *Proc. Natl. Acad. Sci. U.S.A.* **2014**, *111*, 13780–13785.
- (37) Shiraiwa, M.; Ammann, M.; Koop, T.; Pöschl, U. Gas uptake and chemical aging of semisolid organic aerosol particles. *Proc. Natl. Acad. Sci. U.S.A.* **2011**, *108*, 11003–11008.
- (38) Zaveri, R. A.; Shilling, J. E.; Zelenyuk, A.; Zawadowicz, M. A.; Suski, K.; China, S.; Bell, D. M.; Veghte, D.; Laskin, A. Particle Phase Diffusion Modulates Partitioning of Semivolatile Organic Compounds to Aged Secondary Organic Aerosol. *Environ. Sci. Technol.* **2020**, *54*, 2595–2605.
- (39) Riipinen, I.; Pierce, J.; Yli Juuti, T.; Nieminen, T.; Häkkinen, S.; Ehn, M.; Junninen, H.; Lehtipalo, K.; Petäjä, T.; Slowik, J.; et al. Organic condensation: a vital link connecting aerosol formation to cloud condensation nuclei (CCN) concentrations. *Atmos. Chem. Phys.* **2011**, *11*, 3865–3878.
- (40) Murray, B. J.; Wilson, T. W.; Dobbie, S.; Cui, Z.; Al Jumur, S. M.; Möhler, O.; Schnaiter, M.; Wagner, R.; Benz, S.; Niemand, M.; et al. Heterogeneous nucleation of ice particles on glassy aerosols under cirrus conditions. *Nat. Geosci.* **2010**, *3*, 233–237.
- (41) Wagner, R.; Höhler, K.; Huang, W.; Kiselev, A.; Möhler, O.; Mohr, C.; Pajunoja, A.; Saathoff, H.; Schiebel, T.; Shen, X. Heterogeneous ice nucleation of α pinene SOA particles before and after ice cloud processing. *J. Geophys. Res.: Atmos.* **2017**, *122*, 4924–4943.
- (42) Wang, B.; Lambe, A. T.; Massoli, P.; Onasch, T. B.; Davidovits, P.; Worsnop, D. R.; Knopf, D. A. The deposition ice nucleation and immersion freezing potential of amorphous secondary organic aerosol: Pathways for ice and mixed phase cloud formation. *J. Geophys. Res.: Atmos.* **2012**, *117* (D16), DOI: 10.1029/2012JD018063.

- (43) Li, Y.; Day, D. A.; Stark, H.; Jimenez, J.; Shiraiwa, M. Predictions of the glass transition temperature and viscosity of organic aerosols by volatility distributions. *Atmos. Chem. Phys.* **2020**, *20*, 8103–8122.
- (44) Budisulistiorini, S. H.; Nenes, A.; Carlton, A. G.; Surratt, J. D.; McNeill, V. F.; Pye, H. O. Simulating aqueous phase isoprene epoxydiol (IEPOX) secondary organic aerosol production during the 2013 Southern Oxidant and Aerosol Study (SOAS). *Environ. Sci. Technol.* **2017**, *51*, 5026–5034.
- (45) Bateman, A. P.; Gong, Z.; Liu, P.; Sato, B.; Cirino, G.; Zhang, Y.; Artaxo, P.; Bertram, A. K.; Manzi, A. O.; Rizzo, L. V.; et al. Submicrometre particulate matter is primarily in liquid form over Amazon rainforest. *Nat. Geosci.* **2016**, *9*, 34–37.
- (46) Bateman, A. P.; Gong, Z.; Harder, T. H.; Sá, S. S. d.; Wang, B.; Castillo, P.; China, S.; Liu, Y.; O'Brien, R. E.; Palm, B. B.; et al. Anthropogenic influences on the physical state of submicron particulate matter over a tropical forest. *Atmos. Chem. Phys.* **2017**, *17*, 1759–1773.
- (47) Renbaum Wolff, L.; Grayson, J. W.; Bateman, A. P.; Kuwata, M.; Sellier, M.; Murray, B. J.; Shilling, J. E.; Martin, S. T.; Bertram, A. K. Viscosity of α pinene secondary organic material and implications for particle growth and reactivity. *Proc. Natl. Acad. Sci. U.S.A.* **2013**, *110*, 8014–8019.
- (48) Shiraiwa, M.; Seinfeld, J. H. Equilibration timescale of atmospheric secondary organic aerosol partitioning. *Geophys. Res. Lett.* **2012**, *39* (24), DOI: 10.1029/2012GL054008.
- (49) Shrivastava, M.; Cappa, C. D.; Fan, J.; Goldstein, A. H.; Guenther, A. B.; Jimenez, J. L.; Kuang, C.; Laskin, A.; Martin, S. T.; Ng, N. L.; et al. Recent advances in understanding secondary organic aerosol: Implications for global climate forcing. *Rev. Geophys.* **2017**, *55*, 509–559.
- (50) Baltensperger, U.; Prévôt, A. S. Chemical analysis of atmospheric aerosols. *Anal. Bioanal. Chem.* **2008**, *390*, 277–280.
- (51) Pöschl, U.; Shiraiwa, M. Multiphase chemistry at the atmosphere–biosphere interface influencing climate and public health in the anthropocene. *Chem. Rev.* **2015**, *115*, 4440–4475.
- (52) Shiraiwa, M.; Li, Y.; Tsimpidi, A. P.; Karydis, V. A.; Berkemeier, T.; Pandis, S. N.; Lelieveld, J.; Koop, T.; Pöschl, U. Global distribution of particle phase state in atmospheric secondary organic aerosols. *Nat. Commun.* **2017**, *8*, No. 15002.
- (53) Shrivastava, M.; Andreae, M. O.; Artaxo, P.; Barbosa, H. M.; Berg, L. K.; Brito, J.; Ching, J.; Easter, R. C.; Fan, J.; Fast, J. D.; et al. Urban pollution greatly enhances formation of natural aerosols over the Amazon rainforest. *Nat. Commun.* **2019**, *10*, No. 1046.
- (54) Martin, S. T.; Artaxo, P.; Machado, L. A. T.; Manzi, A. O.; Souza, R. A. F. d.; Schumacher, C.; Wang, J.; Andreae, M. O.; Barbosa, H.; Fan, J.; et al. Introduction: observations and modeling of the Green Ocean Amazon (GoAmazon2014/5). *Atmos. Chem. Phys.* **2016**, *16*, 4785–4797.
- (55) Martin, S. T.; Artaxo, P.; Machado, L.; Manzi, A. O.; Souza, R. A. F. d.; Schumacher, C.; Wang, J.; Biscaro, T.; Brito, J.; Calheiros, A.; et al. The Green Ocean Amazon experiment (GoAmazon2014/5) observes pollution affecting gases, aerosols, clouds, and rainfall over the rain forest. *Bull. Am. Meteorol. Soc.* **2017**, *98*, 981–997.
- (56) de Sá, S. S.; Rizzo, L. V.; Palm, B. B.; Campuzano Jost, P.; Day, D. A.; Yee, L. D.; Wernis, R.; Isaacman VanWertz, G.; Brito, J.; Carbone, S.; et al. Contributions of biomass burning, urban, and biogenic emissions to the concentrations and light absorbing properties of particulate matter in central Amazonia during the dry season. *Atmos. Chem. Phys.* **2019**, *19*, 7973–8001.
- (57) Thalman, R.; de Sá, S. S.; Palm, B. B.; Barbosa, H. M. J.; Pöhlker, M. L.; Alexander, M. L.; Brito, J.; Carbone, S.; Castillo, P.; Day, D. A.; Kuang, C.; Manzi, A.; Ng, N. L.; Sedlacek Iii, A. J.; Souza, R.; Springston, S.; Watson, T.; Pöhlker, C.; Pöschl, U.; Andreae, M. O.; Artaxo, P.; Jimenez, J. L.; Martin, S. T.; Wang, J. CCN activity and organic hygroscopicity of aerosols downwind of an urban region in central Amazonia: seasonal and diel variations and impact of anthropogenic emissions. *Atmos. Chem. Phys.* **2017**, *17*, 11779–11801.
- (58) Cirino, G.; Brito, J.; Barbosa, H. M.; Rizzo, L. V.; Tunved, P.; de Sá, S. S.; Jimenez, J. L.; Palm, B. B.; Carbone, S.; Lavric, J. V.; et al. Observations of Manaus urban plume evolution and interaction with biogenic emissions in GoAmazon 2014/5. *Atmos. Environ.* **2018**, *191*, 513–524.
- (59) Andreae, M. O.; Acevedo, O. C.; Araújo, A.; Artaxo, P.; Barbosa, C. G.; Barbosa, H.; Brito, J.; Carbone, S.; Chi, X.; Cintra, B.; et al. The Amazon Tall Tower Observatory (ATTO): overview of pilot measurements on ecosystem ecology, meteorology, trace gases, and aerosols. *Atmos. Chem. Phys.* **2015**, *15*, 10723–10776.
- (60) Chen, Q.; Farmer, D.; Rizzo, L.; Pauliquevis, T.; Kuwata, M.; Karl, T. G.; Guenther, A.; Allan, J. D.; Coe, H.; Andreae, M.; et al. Submicron particle mass concentrations and sources in the Amazonian wet season (AMAZE 08). *Atmos. Chem. Phys.* **2015**, *15*, 3687–3701.
- (61) Rodrigues, M. G. d. A.; Sousa, J. D. d. B.; Dias, A. L. B.; Monteiro, W. M.; Sampaio, V. d. S. The role of deforestation on American cutaneous leishmaniasis incidence: spatial temporal distribution, environmental and socioeconomic factors associated in the Brazilian Amazon. *Trop. Med. Int. Health* **2019**, *24*, 348–355.
- (62) Carreiras, J. M. B.; Jones, J.; Lucas, R. M.; Gabriel, C. Land use and land cover change dynamics across the Brazilian Amazon: insights from extensive time series analysis of remote sensing data. *PLoS One* **2014**, *9*, No. e104144.
- (63) Silva, C. A.; Santilli, G.; Sano, E. E.; Laneve, G. Fire occurrences and greenhouse gas emissions from deforestation in the Brazilian Amazon. *Remote Sens.* **2021**, *13*, No. 376.
- (64) Krieger, U. K.; Marcolli, C.; Reid, J. P. Exploring the complexity of aerosol particle properties and processes using single particle techniques. *Chem. Soc. Rev.* **2012**, *41*, 6631–6662.
- (65) Bilde, M.; Barsanti, K.; Booth, M.; Cappa, C. D.; Donahue, N. M.; Emanuelsson, E. U.; McFiggans, G.; Krieger, U. K.; Marcolli, C.; Topping, D.; et al. Saturation vapor pressures and transition enthalpies of low volatility organic molecules of atmospheric relevance: from dicarboxylic acids to complex mixtures. *Chem. Rev.* **2015**, *115*, 4115–4156.
- (66) Knopf, D. A.; Alpert, P. A.; Wang, B. The role of organic aerosol in atmospheric ice nucleation: a review. *ACS Earth Space Chem.* **2018**, *2*, 168–202.
- (67) Reid, J. P.; Bertram, A. K.; Topping, D. O.; Laskin, A.; Martin, S. T.; Petters, M. D.; Pope, F. D.; Rovelli, G. The viscosity of atmospherically relevant organic particles. *Nat. Commun.* **2018**, *9*, No. 956.
- (68) DeRieux, W. S. W.; Li, Y.; Lin, P.; Laskin, J.; Laskin, A.; Bertram, A. K.; Nizkorodov, S. A.; Shiraiwa, M. Predicting the glass transition temperature and viscosity of secondary organic material using molecular composition. *Atmos. Chem. Phys.* **2018**, *18*, 6331–6351.
- (69) Li, Y.; Pöschl, U.; Shiraiwa, M. Molecular corridors and parameterizations of volatility in the chemical evolution of organic aerosols. *Atmos. Chem. Phys.* **2016**, *16*, 3327–3344.
- (70) Canagaratna, M.; Jimenez, J.; Kroll, J.; Chen, Q.; Kessler, S.; Massoli, P.; Hildebrandt Ruiz, L.; Fortner, E.; Williams, L.; Wilson, K.; et al. Elemental ratio measurements of organic compounds using aerosol mass spectrometry: characterization, improved calibration, and implications. *Atmos. Chem. Phys.* **2015**, *15*, 253–272.
- (71) Donahue, N. M.; Kroll, J.; Pandis, S. N.; Robinson, A. L. A two dimensional volatility basis set—Part 2: Diagnostics of organic aerosol evolution. *Atmos. Chem. Phys.* **2012**, *12*, 615–634.
- (72) Zhao, B.; Shrivastava, M.; Donahue, N. M.; Gordon, H.; Schervish, M.; Shilling, J. E.; Zaveri, R. A.; Wang, J.; Andreae, M. O.; Zhao, C.; et al. High concentration of ultrafine particles in the Amazon free troposphere produced by organic new particle formation. *Proc. Natl. Acad. Sci. U.S.A.* **2020**, *117*, 25344–25351.
- (73) Zhao, B.; Fast, J. D.; Donahue, N. M.; Shrivastava, M.; Schervish, M.; Shilling, J. E.; Gordon, H.; Wang, J.; Gao, Y.; Zaveri, R. A.; Liu, Y.; Gaudet, B. Impact of Urban Pollution on Organic Mediated New Particle Formation and Particle Number Concentration in the Amazon Rainforest. *Environ. Sci. Technol.* **2021**, *55*, 4357–4367.
- (74) Jokinen, T.; Berndt, T.; Makkonen, R.; Kerminen, V. M.; Junninen, H.; Paasonen, P.; Stratmann, F.; Herrmann, H.; Guenther, A. B.; Worsnop, D. R.; et al. Production of extremely low volatile organic compounds from biogenic emissions: Measured yields and atmospheric implications. *Proc. Natl. Acad. Sci. U.S.A.* **2015**, *112*, 7123–7128.

- (75) Schervish, M.; Donahue, N. M. Peroxy radical chemistry and the volatility basis set. *Atmos. Chem. Phys.* **2020**, *20*, 1183–1199.
- (76) Gordon, M.; Taylor, J. S. Ideal copolymers and the second order transitions of synthetic rubbers. I. Non crystalline copolymers. *J. Appl. Chem.* **1952**, *2*, 493–500.
- (77) Slade, J. H.; Ault, A. P.; Bui, A. T.; Ditto, J. C.; Lei, Z.; Bondy, A. L.; Olson, N. E.; Cook, R. D.; Desrochers, S. J.; Harvey, R. M.; Erickson, M. H.; Wallace, H. W.; Alvarez, S. L.; Flynn, J. H.; Boor, B. E.; Petrucci, G. A.; Gentner, D. R.; Griffin, R. J.; Shepson, P. B. Bouncer Particles at Night: Biogenic Secondary Organic Aerosol Chemistry and Sulfate Drive Diel Variations in the Aerosol Phase in a Mixed Forest. *Environ. Sci. Technol.* **2019**, *53*, 4977–4987.
- (78) Saukko, E.; Kuuluvainen, H.; Virtanen, A. A method to resolve the phase state of aerosol particles. *Atmos. Meas. Tech.* **2012**, *5*, 259–265.
- (79) Saukko, E.; Lambe, A. T.; Massoli, P.; Koop, T.; Wright, J. P.; Croasdale, D. R.; Pedernera, D. A.; Onasch, T. B.; Laaksonen, A.; Davidovits, P.; Worsnop, D. R.; Virtanen, A. Humidity dependent phase state of SOA particles from biogenic and anthropogenic precursors. *Atmos. Chem. Phys.* **2012**, *12*, 7517–7529.
- (80) Marsh, A.; Petters, S. S.; Rothfuss, N. E.; Rovelli, G.; Song, Y. C.; Reid, J. P.; Petters, M. D. Amorphous phase state diagrams and viscosity of ternary aqueous organic/organic and inorganic/organic mixtures. *Phys. Chem. Chem. Phys.* **2018**, *20*, 15086–15097.
- (81) Marcolli, C.; Luo, B.; Peter, T. Mixing of the organic aerosol fractions: Liquids as the thermodynamically stable phases. *J. Phys. Chem. A* **2004**, *108*, 2216–2224.
- (82) Martin, S. T. Phase transitions of aqueous atmospheric particles. *Chem. Rev.* **2000**, *100*, 3403–3454.
- (83) Zobrist, B.; Marcolli, C.; Pedernera, D.; Koop, T. Do atmospheric aerosols form glasses? *Atmos. Chem. Phys.* **2008**, *8*, 5221–5244.
- (84) Angell, C. A. Thermodynamic aspects of the glass transition in liquids and plastic crystals. *Pure Appl. Chem.* **1991**, *63*, 1387–1392.
- (85) Gervasi, N. R.; Topping, D. O.; Zuend, A. A predictive group contribution model for the viscosity of aqueous organic aerosol. *Atmos. Chem. Phys.* **2020**, *20*, 2987–3008.
- (86) Fast, J. D.; Gustafson, W. I., Jr.; Easter, R. C.; Zaveri, R. A.; Barnard, J. C.; Chapman, E. G.; Grell, G. A.; Peckham, S. E. Evolution of ozone, particulates, and aerosol direct radiative forcing in the vicinity of Houston using a fully coupled meteorology chemistry aerosol model. *J. Geophys. Res.: Atmos.* **2006**, *111* (D21), DOI: 10.1029/2005JD006721.
- (87) Grell, G. A.; Peckham, S. E.; Schmitz, R.; McKeen, S. A.; Frost, G.; Skamarock, W. C.; Eder, B. Fully coupled “online” chemistry within the WRF model. *Atmos. Environ.* **2005**, *39*, 6957–6975.
- (88) Zaveri, R. A.; Easter, R. C.; Fast, J. D.; Peters, L. K. Model for simulating aerosol interactions and chemistry (MOSAIC). *J. Geophys. Res.: Atmos.* **2008**, *113* (D13), DOI: 10.1029/2007JD008782.
- (89) Guenther, A.; Jiang, X.; Heald, C. L.; Sakulyanontvittaya, T.; Duhl, T.; Emmons, L.; Wang, X. The Model of Emissions of Gases and Aerosols from Nature version 2.1 (MEGAN2. 1): an extended and updated framework for modeling biogenic emissions. *Geosci. Model Dev.* **2012**, *5*, 1471–1492.
- (90) Zhao, C.; Huang, M.; Fast, J. D.; Berg, L. K.; Qian, Y.; Guenther, A.; Gu, D.; Shrivastava, M.; Liu, Y.; Walters, S.; et al. Sensitivity of biogenic volatile organic compounds to land surface parameterizations and vegetation distributions in California. *Geosci. Model Dev.* **2016**, *9*, 1959–1976.
- (91) Berkemeier, T.; Shiraiwa, M.; Pöschl, U.; Koop, T. Competition between water uptake and ice nucleation by glassy organic aerosol particles. *Atmos. Chem. Phys.* **2014**, *14*, 12513–12531.
- (92) Champion, W. M.; Rothfuss, N. E.; Petters, M. D.; Grieshop, A. P. Volatility and Viscosity Are Correlated in Terpene Secondary Organic Aerosol Formed in a Flow Reactor. *Environ. Sci. Technol. Lett.* **2019**, *6*, 513–519.
- (93) Wendisch, M.; Pöschl, U.; Andreae, M. O.; Machado, L. A. T.; Albrecht, R.; Schlager, H.; Rosenfeld, D.; Martin, S. T.; Abdelmonem, A.; Afchine, A.; Araújo, A. C.; Artaxo, P.; Aufmhoff, H.; Barbosa, H. M. J.; Borrmann, S.; Braga, R.; Buchholz, B.; Cecchini, M. A.; Costa, A.; Curtius, J.; Dollner, M.; Dorf, M.; Dreiling, V.; Ebert, V.; Ehrlich, A.; Ewald, F.; Fisch, G.; Fix, A.; Frank, F.; Fütterer, D.; Heckl, C.; Heidelberg, F.; Hüneke, T.; Jäkel, E.; Järvinen, E.; Jurkat, T.; Kanter, S.; Kästner, U.; Kenntner, M.; Kesselmeier, J.; Klimach, T.; Knecht, M.; Kohl, R.; Kölling, T.; Krämer, M.; Krüger, M.; Krisna, T. C.; Lavric, J. V.; Longo, K.; Mahnke, C.; Manzi, A. O.; Mayer, B.; Mertes, S.; Minikin, A.; Molleker, S.; Münch, S.; Nillius, B.; Pfeilsticker, K.; Pöhlker, C.; Roiger, A.; Rose, D.; Rosenow, D.; Sauer, D.; Schnaiter, M.; Schneider, J.; Schulz, C.; de Souza, R. A. F.; Spanu, A.; Stock, P.; Vila, D.; Voigt, C.; Walser, A.; Walter, D.; Weigel, R.; Weinzierl, B.; Werner, F.; Yamasoe, M. A.; Ziereis, H.; Zinner, T.; Zöger, M. ACRIDICON–CHUVA Campaign: Studying Tropical Deep Convective Clouds and Precipitation over Amazonia Using the New German Research Aircraft HALO. *Bull. Am. Meteorol. Soc.* **2016**, *97*, 1885–1908.
- (94) Andreae, M. O.; Afchine, A.; Albrecht, R.; Holanda, B. A.; Artaxo, P.; Barbosa, H. M. J.; Borrmann, S.; Cecchini, M. A.; Costa, A.; Dollner, M.; Fütterer, D.; Järvinen, E.; Jurkat, T.; Klimach, T.; Konemann, T.; Knote, C.; Krämer, M.; Krisna, T.; Machado, L. A. T.; Mertes, S.; Minikin, A.; Pöhlker, C.; Pöhlker, M. L.; Pöschl, U.; Rosenfeld, D.; Sauer, D.; Schlager, H.; Schnaiter, M.; Schneider, J.; Schulz, C.; Spanu, A.; Sperling, V. B.; Voigt, C.; Walser, A.; Wang, J.; Weinzierl, B.; Wendisch, M.; Ziereis, H. Aerosol characteristics and particle production in the upper troposphere over the Amazon Basin. *Atmos. Chem. Phys.* **2018**, *18*, 921–961.
- (95) Kodros, J. K.; Papanastasiou, D. K.; Paglione, M.; Masiol, M.; Squizzato, S.; Florou, K.; Skyllakou, K.; Kaltonoudis, C.; Nenes, A.; Pandis, S. N. Rapid dark aging of biomass burning as an overlooked source of oxidized organic aerosol. *Proc. Natl. Acad. Sci. U.S.A.* **2020**, *117*, 33028–33033.
- (96) Hu, W.; Palm, B. B.; Day, D. A.; Campuzano Jost, P.; Krechmer, J. E.; Peng, Z.; de Sá, S. S.; Martin, S. T.; Alexander, M. L.; Baumann, K.; Hacker, L.; Kiendler Scharr, A.; Koss, A. R.; de Gouw, J. A.; Goldstein, A. H.; Seco, R.; Sjostedt, S. J.; Park, J. H.; Guenther, A. B.; Kim, S.; Canonaco, F.; Prévôt, A. S. H.; Brune, W. H.; Jimenez, J. L. Volatility and lifetime against OH heterogeneous reaction of ambient isoprene epoxydiols derived secondary organic aerosol (IEPOX SOA). *Atmos. Chem. Phys.* **2016**, *16*, 11563–11580.
- (97) May, A. A.; Levin, E. J. T.; Hennigan, C. J.; Riipinen, I.; Lee, T.; Collett, J. L., Jr.; Jimenez, J. L.; Kreidenweis, S. M.; Robinson, A. L. Gas particle partitioning of primary organic aerosol emissions: 3. Biomass burning. *J. Geophys. Res.: Atmos.* **2013**, *118*, 11327–11338.
- (98) Wang, W.; Lei, T.; Zuend, A.; Su, H.; Cheng, Y.; Shi, Y.; Ge, M.; Liu, M. Effect of mixing structure on the water uptake of mixtures of ammonium sulfate and phthalic acid particles. *Atmos. Chem. Phys.* **2021**, *21*, 2179–2190.
- (99) Jathar, S. H.; Mahmud, A.; Barsanti, K. C.; Asher, W. E.; Pankow, J. F.; Kleeman, M. J. Water uptake by organic aerosol and its influence on gas/particle partitioning of secondary organic aerosol in the United States. *Atmos. Environ.* **2016**, *129*, 142–154.